

Chirp Compensation in Active Mode-Locked Semiconductor Diode Laser Using a DFB

by

Susan Bach

Submitted to the
Department of Electrical Engineering and Computer Science
in Partial Fulfillment of the Requirements for the
Degree of

Master of Engineering

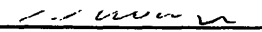
at the

Massachusetts Institute of Technology


September 1994

© Massachusetts Institute of Technology, 1994.
All rights reserved

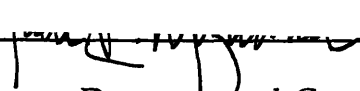
Author

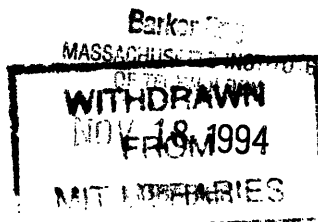

Department of Electrical Engineering and Computer Science
September 14, 1994

Certified by


Hermann A. Haus
Institute Professor
Thesis Supervisor

Accepted by


Frederic R. Morgenthaler
Chairman, Departmental Committee on Graduate Studies



Chirp Compensation in Active Mode-Locked Semiconductor Diode Laser Using a DFB

by

Susan Bach

Submitted to the Department of Electrical Engineering and Computer Science
on September 14, 1994 in Partial Fulfillment of the Requirements for the
Degree of Master of Engineering

Abstract

This thesis investigates the possibility of canceling chirp in an actively mode-locked semiconductor laser using a DFB structure. The chirp is caused by the nonlinearity of the diode, namely, the line-width enhancement factor, α . The mode-locking equations are formed, and the postulated solution is a gaussian pulse shape. The diode is modeled primarily using the rate equations for carrier and photon densities, and the DFB is modeled by transfer matrix theory. Using these models, a program was written to simulate a one-way ring structure. A mathematical analysis of the carrier density, given current and pulse shape, enabled predictions on gain. From these results, the mode-locking equations could be solved, thus defining the pulse uniquely and determining the amount of dispersion necessary for no chirp. Once dispersion was known, the DFB structure could be designed. First, numerical simulations were run with no dispersion and $\alpha=0$ and also $\alpha=5$. These simulations demonstrated that the program works, and that α does produce a significant amount of chirp. Following these results, simulations were run with the DFB designed for three different amounts of dispersion: $D_{fb}=1.2662 \times 10^{-25} \text{s}^2$, $2.5332 \times 10^{-26} \text{s}^2$, and $7.1061 \times 10^{-27} \text{s}^2$. At $D_{fb}=1.2662 \times 10^{-25} \text{s}^2$, where no chirp was calculated, there was very little chirp, but double pulsing was a major problem. At $D_{fb}=2.5332 \times 10^{-26} \text{s}^2$, there was less double pulsing, and the chirp seemed acceptably low. At $D_{fb}=7.1061 \times 10^{-27} \text{s}^2$, there was quite a bit of chirp, however the pulse was clean. It is suggested that the best among the three is $D_{fb}=2.5332 \times 10^{-26} \text{s}^2$ with $\kappa=250 \text{cm}^{-1}$ and $\alpha=5$.

Thesis Supervisor: Professor H. A. Haus
Title: Institute Professor

Acknowledgements

First and foremost, I must thank Professor Haus. This project was his creation and without his help it would have been impossible to complete. His enthusiasm is heartening and contagious and sometimes it is just as fascinating to *watch* him talk as it is to actually *listen*. He sets a standard for honest and ambitious but friendly science which makes the Optics Group a particularly pleasant and productive place to work.

Speaking of the lab, there are definitely others that I am grateful towards. Luc and Farzana were amazingly patient and generous with their time. Luc might be glad not to have me in the office 'assling him anymore, but I think he'll miss it! Farzana and I are "kindred spirits" (keep on Trekkinn!)--thanks for the computer expertise and good conversation. Other people I would like to thank are Jerry, William, Gadi, Chris and, of course, Boris who was always willing to let me bend his ear.

There are two people outside of lab whom I could just hug to death for all their support and friendship. With friends like Audrey and Claudia, there is nothing a person cannot do. This past year has been amazingly difficult and you were there for me. Thank you, thank you, thank you!

Finally, my family. To my brothers, Ralf and Jürgen, you have been the best big brothers a little sister could ask for! I wish you both the best in your present endeavors. And to my parents, well, it is difficult to express so much in words--"Gee, thanks!" just doesn't quite cut it. Each day I understand a little bit better just how much you have done for me and how much you love me, and in learning this, each day I become stronger and more capable of returning that love to you and all those around me.

PS I couldn't just leave without saying something about MIT as a whole. It has been a roller coaster ride through and through. The ups, the downs, the good times and the bad times--I will remember everything like it was yesterday. I am glad I took the ride, and I wish I could take it again. Thank God I can't!

Contents

1 Introduction	8
2 Mode-Locking	10
2.1 Introduction.....	10
2.2 Elements of Active Mode-Locking.....	11
2.2.1 Gain Medium.....	12
2.2.2 Linear Loss.....	14
2.2.3 Linear Phase Shift.....	14
2.2.4 Dispersion.....	14
2.2.5 Time Shift.....	14
2.3 Master Equation and Solution.....	15
2.4 Ring Structure.....	16
3 Semiconductor Lasers	17
3.1 Introduction.....	17
3.2 Gain.....	20
3.3 Rate Equations.....	21
3.4 Refractive Index.....	22
3.4.1 Propagation and Dispersion.....	23
3.4.2 Line-width Enhancement Factor.....	25
4 Distributed Feedback Structures	27
4.1 Introduction.....	27
4.2 DFB Equations.....	28
4.3 Dispersion.....	30
4.4 Matching Structure.....	33
4.5 Coupling Coefficient.....	35

5 Simulation Models	37
5.1 Introduction.....	37
5.2 Simulating the Semiconductor Laser.....	37
5.3 Modeling the DFB.....	40
5.4 Combination Design.....	42
6 Mathematical Analysis	43
6.1 Introduction.....	43
6.2 Carrier Density.....	43
6.3 Mode-Locking.....	45
6.4 Design of the DFB.....	48
7 Results of Simulations	50
7.1 Introduction.....	50
7.2 Testing and Control Simulations.....	53
7.3 Results.....	57
8 Conclusion	62
8.1 Summary of Results.....	62
8.2 Analysis of Results.....	62
8.3 Possible Improvements.....	63
8.4 The End.....	63
A Calculating Parameters of the Pulse and DFB	64
B The Program	68
References	85

List of Figures

2.1	Resonant frequencies of the mode-locking cavity. Each mode has some width due to nonlinearities and phase shifts within the cavity.	11
2.2	Modulation of the gain and constant loss.	13
2.3	Ring model of mode-locked cavity.	16
3.1	Diagram of a semiconductor diode.	17
3.2	Picture of (a) spontaneous emission and (b) stimulated emission.	18
3.3.	Total internal reflection occurs when $n_1 > n_2$ and $\theta_i > \theta_c$.	19
3.4	Gain of the diode over frequency for different carrier densities. The gain increases with increasing carrier density. [1]	21
4.1	A normal waveguide and a DFB structure with sinusoidal perturbations with period Λ .	28
4.2	Second-order dispersion versus $ \delta $ for $\kappa=160$ to 400cm^{-1} .	31
4.3	Third-order dispersion versus $ \delta $ for $\kappa=160$ to 400cm^{-1} .	31
4.4	Ratio of third- to second-order dispersion for 5, 10, and 15ps pulses.	32
4.5	Plot of both positive and negative propagation constants, β , versus δ . The area in the middle is the stop band where β is imaginary.	32
4.6	Matching structure.	33
4.7	Smith chart model following Γ of the matched DFB structure.	34
5.1	Model of diode used for simulations. The diode is divided into sections, each with an independent carrier density, and has field arrays in between.	39
5.2	Modeling the DFB as a two-port system.	40
7.1	Output of the diode. The dashed line is the original pulse, and the solid line is the output with current above threshold.	51
7.2	Output of the DFB structure: solid line is the input pulse, dashed line is the field that traveled through, and dotted is the reflected field.	51
7.3	Output of simulation with a non-bandlimited diode.	52
7.4	Output of simulation with bandlimiting.	52
7.5	Pulse series produced in simulation with both DFB and alpha off.	54

7.6	Frequency spectrum of a single pulse from the above series.	54
7.7	A single pulse from the simulation with both DFB and alpha off.	54
7.8	Phase of the above pulse.	54
7.9	Series of pulses from simulation with alpha off and DFB on.	55
7.10	Section of above series one roundtrip in length.	55
7.11	Phase corresponding to Figure 7.10 .	55
7.12	Series of pulses from simulation with DFB off and alpha on. Sinusoidal line is relative carrier density (not actual values).	56
7.13	Frequency spectrum of a single pulse from the above series.	56
7.14	Single pulse from simulation with DFB off and alpha on.	56
7.15	Phase corresponding to Figure 7.14 .	56
7.16	Series of pulses from simulation with $D_{fb}=1.2662 \times 10^{-25}$ and $a=5$. Sinusoidal line is relative carrier density (not actual values).	58
7.17	Frequency spectrum of a single pulse from the above series.	58
7.18	Single pulse from simulation with $D_{fb}=1.2662 \times 10^{-25}$ and $a=5$.	58
7.19	Phase corresponding to Figure 7.18 .	58
7.20	Series of pulses from simulation with $D_{fb}=2.5332 \times 10^{-26}$ and $a=5$. Sinusoidal line is relative carrier density (not actual values).	60
7.21	Frequency spectrum of a single pulse from the above series.	60
7.22	Single pulse from simulation with $D_{fb}=2.5332 \times 10^{-26}$ and $a=5$.	60
7.23	Phase corresponding to Figure 7.22 .	60
7.24	Series of pulses from simulation with $D_{fb}=7.1061 \times 10^{-27}$ and $a=5$. Sinusoidal line is relative carrier density (not actual values).	61
7.25	Frequency spectrum of a single pulse from the above series.	61
7.26	Single pulse from simulation with $D_{fb}=7.1061 \times 10^{-27}$ and $a=5$.	61
7.27	Phase corresponding to Figure 7.26 .	61

List of Tables

3.1	Typical parameter values for a 1.3 μm diode laser from [3]	19
4.1	Signs of propagation parameters in the four quadrants as referred to in Figure 4.5 .	33
8.1	Summary of values found in simulations.	62

Chapter 1

Introduction

Semiconductor lasers were first realized in 1962. Their small size, around $300\mu\text{m}$, high power, and ease of mass production have made them popular for such uses as CD players and pointers. However, in the case of communication applications, especially in producing ultrashort pulses, semiconductor lasers have undesirable nonlinear characteristics due to changes in the carrier population and frequency dependent gain. These factors cause pulse distortion, cross talk and limit the speed of propagation. [1] When using semiconductor lasers for mode-locking purposes, the cavity must be designed for their nonlinearities.

One undesirable effect of the nonlinearities in diode lasers is a chirped pulse. In this thesis, the use of a distributed feedback structure (DFB) to suppress the chirp of mode-locked pulses will be demonstrated through computer simulation. DFB structures are often used as filters since they have a stop band, however in this case the pass band is being used to manipulate the pulse through dispersion. When mode-locking semiconductor lasers, a certain amount of dispersion in the resonating cavity will prevent the presence of chirp in the steady state pulse. Often, optical fiber is used as the cavity, and the length of the fiber determines the amount of dispersion within the cavity. Some examples show lengths of up to 50 meters. A DFB can do the same thing in one centimeter on a semiconductor chip. There are many advantages to this over using fiber. First, the DFB structure can be fabricated with the diode laser, and second, less energy is lost than would be from focusing the field into the fiber.

The major concern in designing the DFB is the linewidth enhancement factor, or the α parameter, of the diode laser which causes the index of the material to change with gain, hence chirping. Chapters 2 and 3, which cover mode-locking and semiconductor diode lasers, respectively, provide the background knowledge to determine how much dispersion is needed to create a stable non-chirped pulse.

Chapter 4 explains the theory on DFB structures, and from this information in addition to the previous chapters, the DFB can be designed. It will also discuss a special use of DFB's to minimize the amount of reflections.

Computer simulation will be implemented in order to test the above theories and demonstrate graphically a mode-locked pulse resulting from this design. Chapter 5 describes how each part of the diode and DFB is simulated and implemented.

Chapter 6 contains a mathematical analysis of a diode laser, namely the carrier density, to determine the amount of dispersion necessary. These results will determine the values of the parameters of the DFB structure.

Chapter 7 details the results of these simulations.

Finally, Chapter 8 includes a summary of the results will be given and any explanations or further insights. Possible improvements and future developments will be described as well.

Chapter 2

Mode-locking

2.1 Introduction

Mode-locking is the method used to generate short pulses on the order of picoseconds or even femtoseconds in length. As the name implies, the phases of cavity modes are locked with respect to each other so that the sum of the modes renders a pulse usually of gaussian or sech shape. These pulses are used for communication, spectroscopy, etc. There are many approaches and tricks employed to create a mode-locking situation depending on what kind of laser is used and the set-up designed around it. Normally, the goal is to produce a pulse as short as possible with no chirp.

As mentioned above, a mode-locking cavity only supports the resonant frequencies, or modes of the cavity. The frequencies that exist within the cavity are dependent on the length of the cavity. In this case, length is not just the physical length but also depends on the refractive index of the materials within the cavity and is so called the optical length. The higher the index the slower the field propagates through the medium, thus the optical length is larger. The propagation constant of a wave for a linear medium is found from:

$$\beta = \omega n / c \quad (2.1)$$

The following equation is equivalent to traveling with the wave:

$$\omega t - \beta z = 0 \quad (2.2)$$

where z is distance. From (2.2), a cavity of length L has an effective length of nL . For a frequency to exist within the cavity, the optical length must be a multiple of half wavelengths in the medium.

$$\frac{m\lambda}{2} = nL \quad (2.3)$$

So the modes in the cavity have frequencies of:

$$f_m = \frac{c}{\lambda} = \frac{mc}{2nL} \quad \text{and} \quad \Delta f = \frac{c}{2nL} \quad (2.4)$$

where m is the mode number. Because the cavity is composed of different media, the refractive index will not be constant throughout the cavity. Thus it is easier to express the mode spacing, $\Delta\omega$, as $2\pi/T_R$ where T_R is the roundtrip time of the cavity.

Ideally, there should be an impulse in the frequency spectrum for each mode at the appropriate frequency, however, realistically, the mode always has some width meaning that there is some energy in the frequencies close to the modal frequencies (Figure 2.1). This is due to noise.

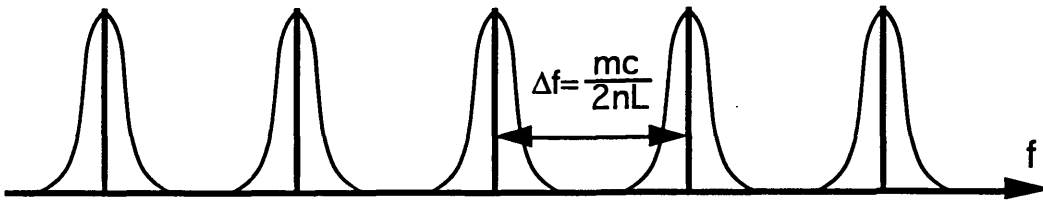


Figure 2.1. Resonant frequencies of the mode-locking cavity. Each mode has some width due to nonlinearities and phase shifts within the cavity.

Future figures of frequency spectrums may not show the individual modes but only an envelope. In a mode-locking situation, these modes sum up to form a pulse in the time domain, the shape of which is dependent on the effect of all the components within the cavity on each mode.

2.2 Elements of Active Mode-Locking

This section will explain all the parts of the master equation for active mode-locking. There are two approaches to analyzing and finding a solution for a mode-locking equation, frequency and time. Mode-locking has both frequency and time dependent parts, but it is generally easier to understand in the time domain. It is also easier to find a solution in the time domain because the equation corresponds to the one-dimensional Schroedinger equation of a particle in a potential well [2]. Thus the known solutions to this equation can also be used for mode-locking.

The effect of each element within the cavity is slight. If exponential, the exponent with a small argument can be expanded and approximated in time as:

$$e^x = 1 + x + \frac{x^2}{2!} + \frac{x^3}{3!} + \dots \approx 1 + x \quad (2.5)$$

Following is a descriptive list each element required for mode-locking already in the form of "x".

2.2.1 Gain Medium

The main active mode-locking element is the gain. In semiconductor diodes, the gain is determined mostly by the injection current. More current means higher gain. Other lasers obtain energy from pump lasers--the more intensity the pump laser provides the higher the gain of the mode-locked laser. In either case, modulating the power source will cause modulation of the gain at the same frequency. For diode lasers, the relation between current and gain is linear but delayed, thus the peak of the current and the peak of the gain (or rather carrier density) do not coincide. The current should be modulated around some threshold value above which there is net gain and below which there is absorption (Figure 2.2). The modulation frequency, ω_m , of the current should correspond to the roundtrip time of the cavity, ie should be equal to the mode spacing $2\pi/T_R$, in order to drive the adjacent modes.

The gain, however, is also frequency dependent, and can be modeled with a lorentzian shape:

$$g(\omega) = \frac{g_o}{1 + \left(\frac{\omega - \omega_o}{\omega_g}\right)^2} \quad (2.6)$$

where g_o is the small signal gain at the center frequency and ω_g is the linewidth of the gain. The center frequency of the field within a mode-locking cavity is the resonant frequency closest to the center frequency of the gain medium. The above equation can be approximated as:

$$g(\omega) \approx g_o \left(1 - \left(\frac{\omega - \omega_o}{\omega_g}\right)^2\right), \quad (2.7)$$

and in the time domain this becomes:

$$g(t) = g_o \left(1 + \frac{1}{\omega_g^2} \frac{d^2}{dt^2}\right) \quad (2.8)$$

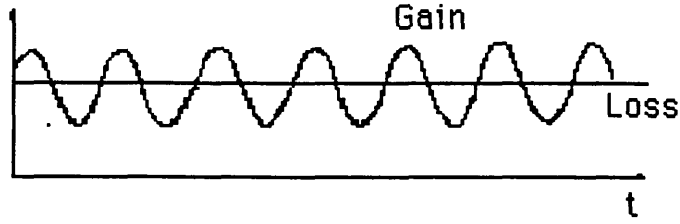


Figure 2.2. Modulation of the gain and constant loss.

The effect of the gain is expressed as:

$$G(t) = g_o \left(M(t) + \frac{1}{\omega_s^2} \frac{d^2}{dt^2} \right) \quad (2.9)$$

where $M(t)$ is the modulation of the gain.

Another gain related element necessary for mode-locking is saturation of the gain. The presence of photons depletes the carrier density, thus increasing intensity decreases the gain. In the initial transient state, the intensity of the pulse increases until enough saturation occurs to achieve steady-state. The relaxation time of the gain medium should be short enough for it to recover within the roundtrip time. The effect of saturation is expressed as:

$$-S(t) \quad (2.10)$$

Semiconductor lasers are unique in that they have a nonlinearity due to the linewidth enhancement factor, α (also to be further explained in chapter 2). It is a gain dependent factor in which the index changes with gain.

$$j\alpha(G(t) - S(t)) \quad (2.11)$$

This element creates difficulties in mode-locking because it induces chirping and instability. When designing the mode-locking cavity, it is important to consider this factor and to counter it with another element such as dispersion.

Another frequency dependent factor is dispersion. The gain medium may have a negligible amount of dispersion compared to the amount experienced within the rest of the cavity, but it is mentioned here since it is included in future calculation and because it does exist. The effect of dispersion, which will be explained in greater detail in Chapter 2, is given by:

$$-jD_d(\omega - \omega_o)^2 \Rightarrow jD_d \frac{d^2}{dt^2} \quad (2.12)$$

where D_d is half the second-derivative of the propagation constant times the length of the diode.

2.2.2 Linear Loss

Somewhere in the cavity the optical field will experience a linear loss, $-L$. The cause of this would be the output coupler, and also loss occurs when the field travels from one medium to another. Possibly, the medium itself will have some amount of loss.

2.2.3 Linear Phase Shift

In the steady state, the pulse after one round trip should be the same as it was before. However, there will be a difference in phase since propagation through a medium adds a phase shift. This is acceptable as long as the difference remains constant between consecutive pulses. The phase shift, $j\psi$, has no shaping effect on the pulse, and only occurs as a result of satisfying the requirements for steady-state.

2.2.4 Dispersion

Dispersion in the diode was already mentioned, but there is also a significant amount of dispersion in the rest of the cavity. Actually, in this case there has to be to compensate for the nonlinearity in the diode. The object of this thesis is to design a DFB structure with the right amount of dispersion to prevent pulse-spreading and chirping caused by the diode. The DFB dispersion is expressed as:

$$-jD_{fb}(\omega - \omega_o)^2 \Rightarrow jD_{fb} \frac{d^2}{dt^2} \quad (2.13)$$

where D_{fb} is half the second derivative of the DFB propagation constant times the length of the DFB.

2.2.5 Time Shift

As the pulse travels through the diode, it experiences a pushing effect causing delay or advancement depending on where the peak of the pulse is with respect to the peak of the gain. So, if the peak of the pulse comes after the peak of gain, the pulse will be "pushed" ahead in time because the front part of the pulse experiences more gain than the later part. This effect is represented by:

$$\delta T \frac{d}{dt} \quad (2.14)$$

That concludes the elements of mode-locking. The next step is to formulate a master equation which will define the pulse.

2.3 Master Equation and Solution

The previous section described every single effect experienced by the pulse in one round trip. The total effect can be expressed in a single equation:

$$a \exp(\delta T \frac{d}{dt} + j\Psi) = a \exp((G(t) - S(t))(1 + j\alpha) - L + jD_d \frac{d^2}{dt^2} + jD_{fb} \frac{d^2}{dt^2}) \quad (2.15)$$

where a is the pulse envelope. Both sides of (2.15) represent the pulse after one round trip. (2.15) can be simplified using (2.5):

$$\delta T \frac{d}{dt} + j\Psi = (G(t) - S(t))(1 + j\alpha) - L + jD_d \frac{d^2}{dt^2} + jD_{fb} \frac{d^2}{dt^2} \quad (2.16)$$

The ansatz for this equation is a gaussian shaped pulse:

$$a = |A| \exp\left(\frac{-t^2}{2\tau^2}(1 + j\beta_c)\right) \exp(-j\Delta\omega t) \quad (2.17)$$

where $|A|$ is the amplitude, τ determines the pulse width, β_c is the chirp parameter, and $\Delta\omega$ is the frequency shift. Applying this solution to (2.16) and separating it into parts by powers of t should render six real equations. For a given cavity, the unknowns of the master equations are the pulse parameters of eq (2.17) as well as ψ and δT . Thus with six unknowns and six equations, the pulse can be defined uniquely.

In chapter 6, the six equations will be worked out explicitly once an analytical model of the gain has been written.

2.4 Ring Structure

This thesis will simulate a ring structure. In this model, **Figure 2.3**, the field travels only in one direction and passes through each medium once in one round trip. To insure that the field propagates only in one direction, an isolator is modelled just before the diode. This isolator passes any field travelling in the clockwise direction and absorbs any field propagating in the opposite direction. Of course, this is pretty idealistic, but any loss from the isolator can be included in the linear loss term above. However, isolators today are pretty good in absorbing the counter propagating fields so this model is not far from reality.

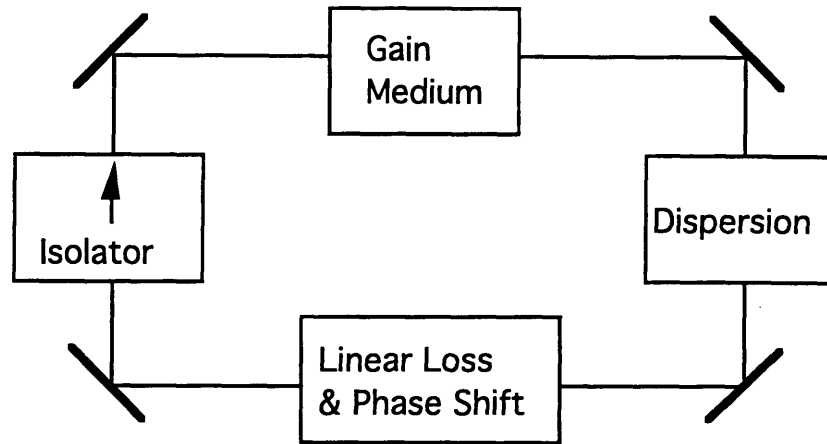


Figure 2.3. Ring model of mode-locked cavity.

This does not mean there will be no counter-propagating waves. The field will be partially reflected by the DFB structure causing backward propagating waves to travel through the diode even with the matching structure to be described in Chapter 4. If the amplitude of these waves is significant, they will deplete the gain medium. This effect must also be included when simulating the diode.

The ring model overall is much easier to simulate than a cavity structure in which the field is reflected back and forth and experiences each effect twice as much but at different times. Also, when fields travel in both directions in the diode, standing waves form, causing spatial hole burning, and some parts of the diode are completely depleted of carriers. This phenomenon is rather difficult to simulate and is a under great deal of study--i.e. too much to think about here.

Chapter 3

Semiconductor Lasers

3.1 Introduction

Semiconductor lasers are made by laying a p-type semiconductor material on an n-type material. At the boundary of the two layers, the p-n junction, electrons diffuse a short distance into the p side from the n side, and holes diffuse into the n side from the p side. The diffusion process reaches a steady state when the resulting charged donors on either side form a field resisting further change in hole/electron populations. Applying a positive voltage across the p-n junction, or forward biasing the diode, will weaken this field allowing more electrons and holes to diffuse into the area around the p-n junction. This area, where both electrons and holes exist near the junction, is called the active region and is the most interesting part of the diode since it is where the optical field travels and experiences gain and loss.

Recombination of the electron and holes in the active region results in an emission of radiative or nonradiative energy. Radiative energy is in the form of photons whose frequency must satisfy the condition: $h\nu = E_g$, where E_g

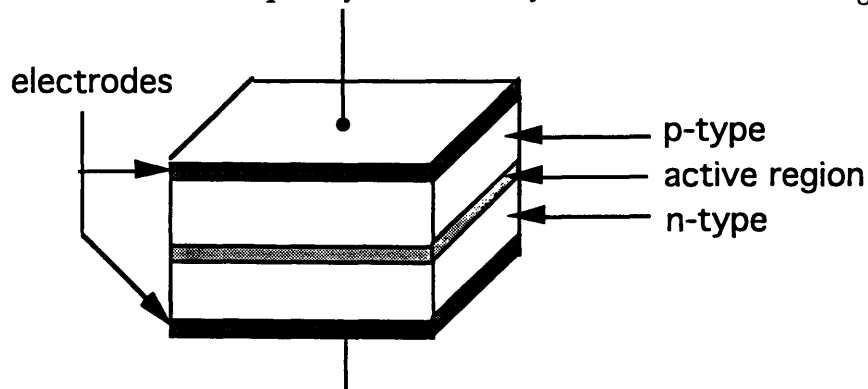


Figure 3.1. Diagram of a semiconductor diode.

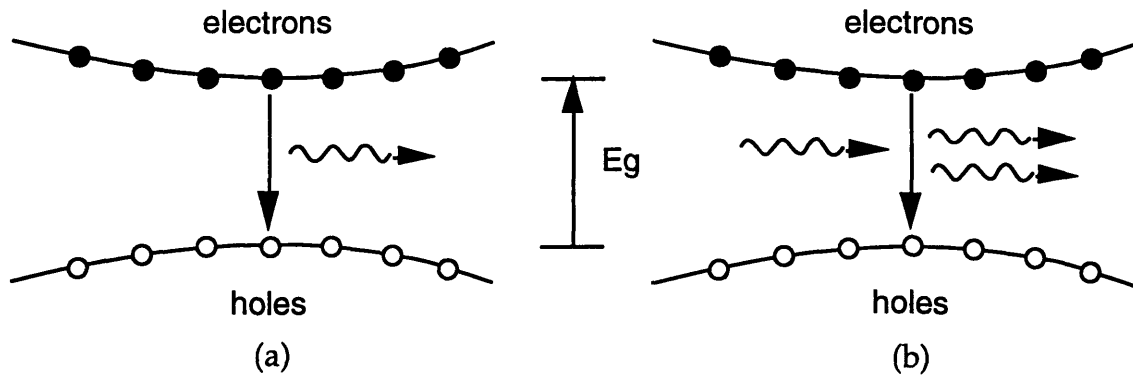


Figure 3.2. Picture of (a) spontaneous emission and (b) stimulated emission.

is the gap energy emitted. The upper energy state of a free electron is called the conduction band while the lower state of a recombined electron/hole pair is the valence band. E_g is the difference in energy between these two states. A recombined electron/hole pair can also absorb this amount of energy and free the electron.

As stated before, forward biasing the diode increases the number of electrons and holes diffusing into the active region. There is a threshold value for the voltage beyond which there is population inversion. The result is the rate of recombination is higher than the reverse process which means that there is more emission than absorption. Thus the optical field experiences gain.

Photon emission from recombination is either spontaneous or stimulated. A spontaneous emission occurs when an electron randomly decays from the conduction band to the valence band, releasing energy. Stimulated emission occurs when another photon induces the electron to decay and release another photon. The photon radiated by the stimulated emission will match the first photon in frequency and direction. Thus the light emitted by the laser will be mostly coherent.

The active region is so designed that its refractive index is slightly higher than that of the surrounding p- or n-type material. Thus, the active region of the diode laser acts like a waveguide, one with gain and absorption, and the light is contained. The mechanism of containment begins with the difference in index. Because the index of the active region is higher, total internal reflection occurs if the field hits the boundary with an angle of incidence greater than the critical angle given by Snell's Law. The critical

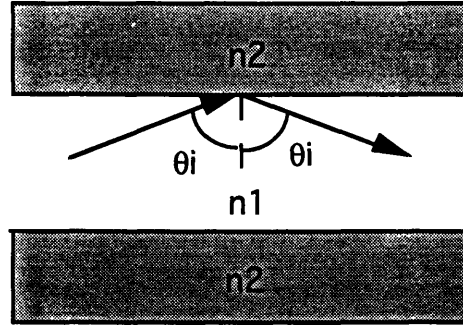


Figure 3.3. Total internal reflection occurs when $n_1 > n_2$ and $\theta_i > \theta_c$.

angle, θ_c , of the incident wave, θ_i , is such that $\sin \theta_t$, the transmitted field angle, is > 1 . (n_1 is the index of the active region; n_2 is the index outside.)

$$\frac{n_1}{c} \sin \theta_i = \frac{n_2}{c} \sin \theta_t \Rightarrow \theta_c = \sin^{-1} \frac{n_2}{n_1} \quad (3.1)$$

The energy of any field traveling almost parallel to the edge of the active region will be totally reflected.

Table 3.1 Typical parameter values for a 1.3 μm diode laser from [3]

Parameter	Symbol	Value
Cavity length	L	250 μm
Active-region width	w	2 μm
Active-layer thickness	d	0.2 μm
Confinement factor	Γ	0.3
Effective mode index	μ	3.4
Group refractive index	μ_g	4
Line-width enhancement factor	α	5
Facet loss	α_m	45 cm^{-1}
Internal loss	α_{int}	40 cm^{-1}
Gain constant	g_0	$2.5 \times 10^{-16} \text{ cm}^2$
Carrier density at transparency	N_t	$1 \times 10^{18} \text{ cm}^{-3}$
Nonradiative recombination rate	A_{nr}	$1 \times 10^8 \text{ s}^{-1}$
Radiative recombination coeff	B	$1 \times 10^{-10} \text{ cm}^3/\text{s}$
Auger recombination coeff	C	$3 \times 10^{-29} \text{ cm}^6/\text{s}$
Threshold carrier population	N_{th}	2.14×10^8
Threshold current	I_{th}	15.8 mA
Carrier lifetime at threshold	τ_e	2.2 ns
Photon lifetime	τ_p	1.6 ps

Table 3.1 lists the important parameters of a semiconductor diode and their characteristic values. These are the actual values used for simulations on the computer.

3.2 Gain

As stated earlier, the field experiences gain when an electron decays from an upper state to a lower state, imparting another photon to the field. If the density of electrons in the conduction band is high and the density of holes in the valence band is also high, then the field will see a net gain since the probability of a stimulated emission is higher than that of a stimulated absorption. Conversely, if the density of the valence band is higher, the field will be absorbed. So far, only two states have been mentioned to simplify explanations. However, each state is actually comprised of many energy levels with a minimum energy gap separating the two states. An electron in one of the upper levels can settle into any of the lower levels, thus varying the amount of energy released. Therefore, the photons emitted are of different frequencies ($E=h\nu$), so the diode can support a limited frequency bandwidth.

It is possible to calculate the probability of the state of each electron and thus estimate the electron density in all the energy levels. The equations involved are too complicated and beyond this thesis to discuss here, however, given the total carrier density, temperature, and diode specifications the gain can be predicted for a range of frequencies.

Figure 3.4 shows a typical gain curve for a semiconductor diode versus a range of energy above the band gap energy. Obviously, frequencies with energy below the band gap energy will experience no gain or absorption because there is no electron transition with that amount of energy. Also, because the probability that an electron will inhabit a very high energy level is very low unless the total carrier density is large, absorption is more likely than gain at higher frequencies. This leaves a band of frequencies for which the optical field will experience gain. The bandwidth is normally on the order of terahertz and the diode is usually designed so that the band centers around 1.3 or 1.5 μm which is where optical fibers have low loss and low dispersion. The simulations in this thesis are for a 1.3 μm diode laser.

The main value needed to simulate the diode is the differential gain. As can be seen from the figure, the gain varies with carrier density. dg/dN

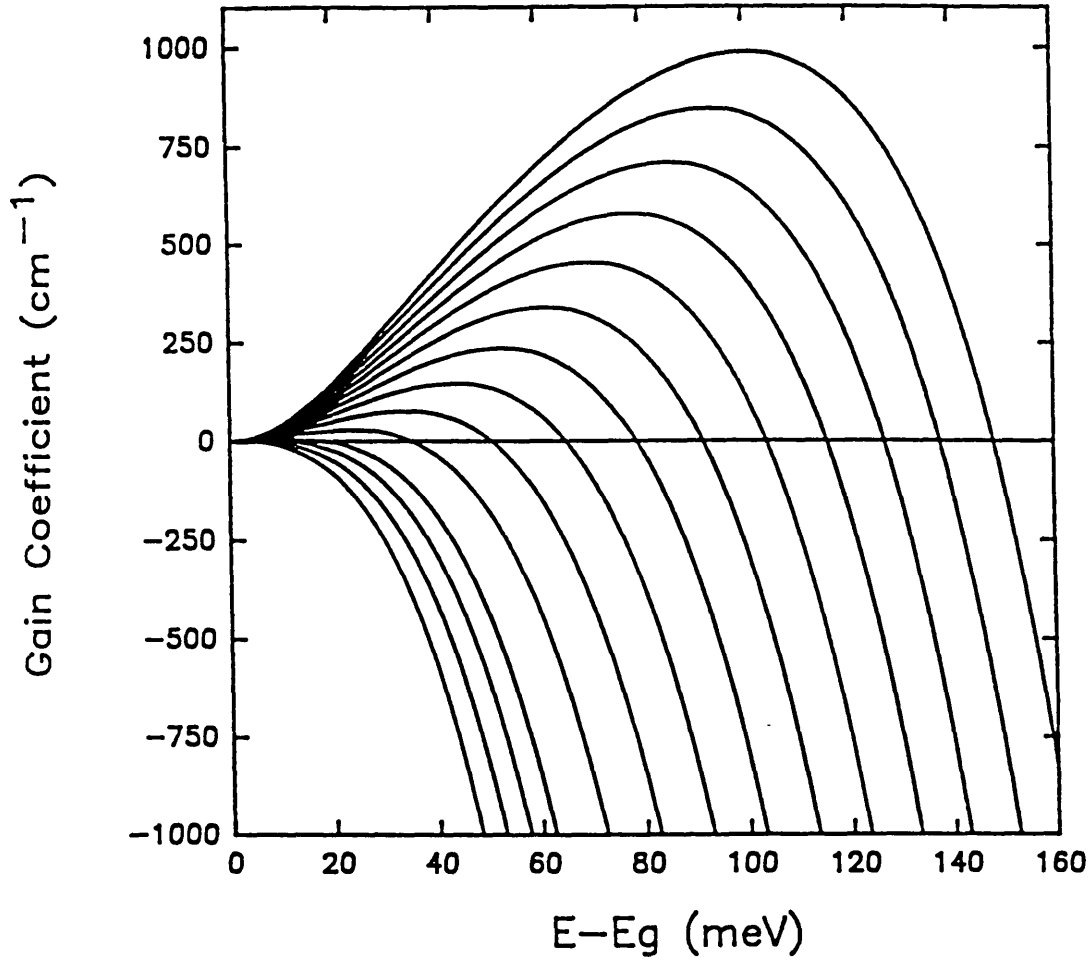


Figure 3.4. Gain of the diode over frequency for different carrier densities. The gain increases with increasing carrier density. [1]

can be approximated and used to create simple equations to estimate the gain of the diode.

3.3 Rate Equations

The carrier and photon density within the active region of the diode can be modeled by two simple first order rate equations as given in [1].

$$\frac{dN}{dt} = \frac{I}{qV} - \frac{N}{\tau_e} - g_o v_g (N - N_t) P \quad (3.2)$$

$$\frac{dP}{dt} = \frac{-P}{\tau_p} + \Gamma g_o v_g (N - N_t) P + \frac{\beta_{sp} N}{\tau_e} \quad (3.3)$$

where N is the carrier density, P is the photon density, I is the current, q is electron charge, V is the volume of the active region, τ_e is the carrier life time, g_o is the differential gain (dg_o/dN), v_g is the group velocity, N_t is the carrier

density at transparency, Γ is the confinement factor, β_{sp} is the spontaneous emission factor, and τ_p is the photon lifetime. The factor τ_p includes internal absorption, mode absorption and scattering loss.

If the carrier density is not above the density at transparency, then there is absorption instead of gain. The carrier density threshold at which the signal starts to experience total gain, not including spontaneous emissions, is found at steady state from [3]:

$$\frac{1}{\tau_p} = \Gamma g_o v_g (N - N_t) \Rightarrow N_{th} = \frac{1}{\tau_p \Gamma g_o v_g} + N_t. \quad (3.4)$$

The current necessary to achieve the carrier density threshold is estimated by setting dN/dt and dP/dt to zero, solving for P in (3.3) and substituting into (3.2). I_{th} is normally defined in the limiting case of $\beta_{sp}=0$ [3].

$$I_{th} = \frac{qV}{\tau_e} N_{th} \quad (3.5)$$

When the current is below threshold, the photon density is very small. Thus, the carrier density can be estimated from (3.2):

$$N = \frac{I\tau_e}{qV} \quad (3.6)$$

These equations are the most important to modeling the gain medium for computer simulation as will be shown in later chapters. Not only do the above equations serve to estimate the gain but also to estimate the carrier density for nonlinear effects, namely involving changes in the refractive index.

3.4 Refractive Index

In a dielectric medium, the presence of an electric field induces dipole action within the material causing a polarization density dependent on the strength of the electric field. Thus, the total electric displacement, D , is given by:

$$D = \epsilon_0 E + P \quad (3.7)$$

where P is the polarization density, E is the electric field and ϵ_0 is the dielectric constant of free space. The polarization density is given by

$$P = \epsilon_0 \chi_e E \quad (3.8)$$

where χ_e is the electric susceptibility tensor. Thus the total dielectric constant of the medium is

$$\epsilon = \epsilon_0 (1 + \chi_e) = n^2 \epsilon_0 \quad (3.9)$$

The dielectric constant is also expressed through the refractive index, n .

$$\epsilon = n^2 \epsilon_0 \Rightarrow n = \sqrt{\frac{\epsilon}{\epsilon_0}} = \sqrt{1 + \chi_e} \quad (3.10)$$

For isotropic mediums, χ_e is a scalar, but for semiconductor material like InGaAsP, the susceptibility tensor is frequency dependent and complex. The next two sections will discuss how each of these traits plays a role in the propagation of electric fields.

3.4.1 Propagation and Dispersion

The propagation constant of a medium partially describes what happens to a field as it moves through the medium and serves as a relation between time and space

$$a(z,t) = F^{-1}(a(z=0, \omega) e^{-j\beta(\omega)z}) \quad (3.11)$$

where $a(z,t)$ is the field envelope in time. For a normal waveguide structure

$$\beta(\omega) = \frac{\omega n}{c} \quad \text{and} \quad c = \frac{1}{\sqrt{\mu \epsilon_0}} \quad (3.12)$$

where c is the speed of light in free space. The above propagation constant can be expanded into a Taylor series around the carrier frequency (ω_0) in order to more easily appreciate its effect on the field:

$$\beta(\omega) = \beta(\omega_0) + \frac{\partial \beta}{\partial \omega} (\omega - \omega_0) + \frac{1}{2} \frac{\partial^2 \beta}{\partial \omega^2} (\omega - \omega_0)^2 + \frac{1}{3!} \frac{\partial^3 \beta}{\partial \omega^3} (\omega - \omega_0)^3 \quad (3.13)$$

The first term is merely a phase shift seen at all frequencies, and $\omega_0/\beta(\omega_0)$ is the phase velocity. The second term is the travel term since $1/\partial\beta/\partial\omega_0$ is v_g , the group velocity. This term describes the speed at which the field's envelope travels. For a nondispersive medium where n is constant, the phase and group velocities are equal, and the rest of the terms are zero. However, semiconductor material has a refractive index dependent on frequency

$$\frac{\partial \beta}{\partial \omega} = \frac{n(\omega_0)}{c} + \frac{\omega_0}{c} \frac{dn(\omega)}{d\omega} \quad (3.14)$$

The third term of the series is first order dispersion present in semiconductor material. The presence of this term means that some frequencies travel faster than others. As a result, the signal experiences chirping as it travels through the medium where

$$\delta_o = l \frac{\partial^2 \beta}{\partial \omega^2} \quad (3.15)$$

is the chirp parameter. For "normal" dispersion, $\partial^2\beta/\partial\omega^2>0$, thus the group velocity of higher frequencies is smaller than that of lower frequencies. In a traveling pulse, the lower frequencies will end up at the front of the pulse ahead of the higher frequencies. The opposite is true for "anomalous" dispersion where $\partial^2\beta/\partial\omega^2<0$.

A pulse traveling in dispersive medium will eventually experience spreading and distortion. One can reverse these effects by propagating the pulse through a medium of opposite dispersion of length such that the chirp parameter cancels that of the first medium. Another trick is to prechirp the pulse before traveling through the medium, however, this requires prior knowledge of the length of the medium.

The fourth term is third order dispersion; the fifth term is fourth order, and so on. The propagation constant is normally assumed to vary slowly enough with frequency that any term after the second derivative is too small to be of significance.

Therefore, in order to simulate the propagation of a field through the diode, the first and second derivatives only of the propagation constant must be known for the carrier frequency of the diode. The first derivative is often expressed simply as:

$$\frac{\partial\beta}{\partial\omega} = \frac{1}{v_g} = \frac{n_g}{c} \quad (3.16)$$

where v_g is the group velocity and n_g is the group index found from (3.14)

$$n_g = n(\omega_o) + \omega_o \frac{dn(\omega)}{d\omega} \Big|_{\omega_o} \quad (3.17)$$

The group refractive index can be measured experimentally by estimating the roundtrip time within the diode cavity, or it can be estimated through detailed calculations not explained here. Values given for the group index for diode laser with a center wavelength of 1.3 μm range between 3 and 4.

The dispersion factor is often given in terms of wavelength instead of frequency because it is easier to measure with respect to wavelength. The conversion is simple since

$$\lambda = \frac{2\pi c}{\omega} \Rightarrow \frac{d\lambda}{d\omega} = -\frac{2\pi c}{\omega^2} \quad (3.18)$$

The dispersion factor is found by taking the derivative of the group velocity with respect to wavelength

$$\frac{\partial}{\partial \lambda} \frac{1}{v_g} = \frac{1}{c} \frac{\partial n_g(\lambda)}{\partial \lambda} \quad (3.19)$$

$$\text{where } n_g(\lambda) = n(\lambda) - \lambda \frac{\partial n(\lambda)}{\partial \lambda} \quad \text{thus} \quad \frac{\partial n_g}{\partial \lambda} = -\lambda \frac{\partial^2 n(\lambda)}{\partial \lambda^2}$$

This last term on the right side of (3.19) is found by measuring the differences in roundtrip times for different wavelengths [1] :

$$\frac{dt_r}{d\lambda} = \frac{2l}{c} \frac{\partial n_g}{\partial \lambda} \quad (3.20)$$

Once the value for $dn_g/d\lambda$ is known, it can be converted in terms of frequency to find $d\beta/d\omega$:

$$\frac{\partial^2 \beta}{\partial \omega^2} = \frac{1}{c} \frac{\partial n_g}{\partial \omega} = \frac{1}{c} \frac{\partial n_g}{\partial \lambda} \frac{d\lambda}{d\omega} = -\frac{2\pi}{\omega^2} \frac{\partial n_g}{\partial \lambda} \quad (3.21)$$

and finally

$$\frac{\partial^2 \beta}{\partial \omega^2} = -\frac{2\pi}{\omega^2} \left(-\lambda \frac{\partial^2 n(\lambda)}{\partial \lambda^2} \right). \quad (3.22)$$

Values given for $dn_g/d\lambda$ were around $-6\mu\text{m}^{-1}$ for a $1.3\mu\text{m}$ laser, thus the dispersion factor used in simulations was $\beta'' = 8.96 \times 10^{-25}$.

3.4.2 Line-width Enhancement Factor

The susceptibility tensor of semiconductor diode lasers is also complex. The imaginary part of the index is also expressed as gain. As gain changes with the varying amount of carrier density shown earlier in this chapter, so too does the imaginary part of the index. In addition, there is a corresponding change in the real part of the refractive index. This variance of index was initially studied by C. H. Henry [4]. It is a nonlinearity of the diode which causes broadening of the pulse and bandwidth and instabilities in mode-locking [5].

The refractive index has a base value from which it varies expressed thus:

$$n = n_b + \Delta n' - j\Delta n'' \quad (3.23)$$

The propagation constant also changes with index:

$$\beta = (\beta_o + \Delta\beta' - j\Delta\beta'') = \frac{\omega}{c} (n_b + \Delta n' - j\Delta n'') \quad (3.24)$$

$$\text{where } \beta_o = \frac{\omega}{c} n_b \Rightarrow \Delta\beta' - j\Delta\beta'' = \frac{\omega}{c} (\Delta n' - j\Delta n'')$$

Gain and the imaginary part of the refractive index are related by:

$$e^{\beta z} = e^{-2\Delta\beta'' z} \quad (3.25)$$

where the gain is assumed to be applied to intensity. Thus, change in the imaginary part is:

$$\Delta n'' = -\frac{g}{2} \frac{c}{\omega} \quad (3.26)$$

The real and imaginary parts of the dielectric constant can be related by Kramer Kronigs relation. However, this is a rather complicated relation and expresses a dependence on frequency. A much simpler relation is given by the linewidth enhancement factor which is the ratio of the change in the real part to the change in the imaginary part [4]:

$$\alpha = \frac{\Delta n'}{\Delta n''} \quad (3.27)$$

It is an approximation which will make mode-locking equations far easier to handle--well worth any loss of accuracy.

Finally, the change in the real part of the refractive index can be expressed in terms of the change in gain:

$$\Delta n' = -\alpha \frac{g}{2} \frac{c}{\omega} \quad (3.28)$$

Values for α are usually between 4 and 6 [4]. So the effect on the signal can be expressed as:

$$ae^{-j\frac{\omega}{c}\Delta n'} = ae^{j\alpha\frac{g(t)}{2}} \approx a(1 + j\alpha\frac{g(t)}{2}) \quad (3.29)$$

Note that this effect is time dependent, and it will be a consideration when simulating the diode. It will be stated in Chapter 5 how this problem was dealt with.

Chapter 4

Distributed Feedback Structures

4.1 Introduction

Most waveguide couplers can only couple waves moving in the same direction since it is necessary that the propagation constants of the two waves are similar for coupling to occur. Distributed feedback structures, however, can couple waves moving in opposite directions. DFB structures are waveguides with periodic perturbations which cause reflections that couple with the opposite wave.

In an unperturbed waveguide, there is no coupling and the propagation of the forward, a , and backward, b , waves are described simply by:

$$\frac{da}{dz} = -j\beta a \quad (4.1)$$

$$\frac{db}{dz} = j\beta b \quad (4.2)$$

In a DFB structure, the waves are modulated by the periodic perturbations, thus the field acquires sidebands called space harmonics. If these side bands have propagation constants similar to the oppositely traveling field in the waveguide, then coupling will occur between the sideband and the oppositely traveling wave.

If the DFB is long enough, there is total reflection of a band of frequencies. The center of this bandwidth is the frequency at which when modulated by the perturbations, the reflected sidebands have the opposite propagation constant. Thus the DFB structure can be used to filter out these frequencies. However, this is not the purpose the DFB will serve for this project, and it is better in this case to avoid the stop band.

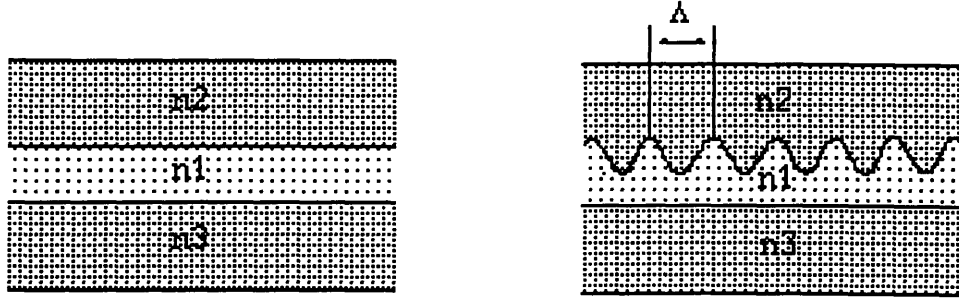


Figure 4.1. A normal waveguide and a DFB structure with sinusoidal perturbations with period Λ .

The DFB shall be used for its dispersion to compensate for the dispersion and nonlinearities in the diode. The propagation constant and thus the dispersion parameter are determined by the coupling coefficient and the periodicity of the perturbations. Since the easiest structure to analyze has sinusoidal perturbation, following is a derivation of the coupling equations and dispersion parameters for such a structure.

4.2 DFB Equations

With sinusoidal perturbations, both backward and forward waves are spatially modulated by $\cos(2\pi/\Lambda)z$, where Λ is the periodicity of the perturbation. Using the forward wave as an example, the side bands would be:

$$a \cos(2\pi/\Lambda) = \frac{A}{2} \left[\exp(-j(\beta - \frac{2\pi}{\Lambda})z) + \exp(-j(\beta + \frac{2\pi}{\Lambda})z) \right] \quad (4.3)$$

If $\beta - \pi/\Lambda$ is close to $-\beta$, the propagation constant of the backward wave, then this sideband will couple with the backward wave as long as

$$|-\beta - (\beta - \frac{2\pi}{\Lambda})| < \pi \quad (4.4)$$

at which point the sideband is no longer coherent with the backward wave and no coupling occurs. It is assumed that the propagation constant of the other sideband ($\beta + 2\pi/\Lambda$) differs too greatly for coupling to occur. Thus propagation of both forward and backward waves can be described by including the coupling of these sidebands:

$$\frac{da}{dz} = -j\beta a + \kappa_{ab} b e^{-j(2\pi/\Lambda)z} \quad (4.5)$$

$$\frac{db}{dz} = j\beta b + \kappa_{ba} a e^{j(2\pi/\Lambda)z} \quad (4.6)$$

where κ is the coupling coefficient determined by the strength of the grating. Note that if $\kappa=0$, the above equation would again describe propagation through a normal waveguide. (4.5-6) can be simplified by removing the fast spatial dependences by substituting the following for a and b :

$$a = A(z)e^{-j(\pi/\Lambda)z}, \quad b = B(z)e^{j(\pi/\Lambda)z} \quad (4.7)$$

The resulting propagation equations from (4.5-7) are:

$$\frac{dA}{dz} = -j\left(\beta - \frac{\pi}{\Lambda}\right)A + \kappa_{ab}B \quad (4.8)$$

$$\frac{dB}{dz} = j\left(\beta - \frac{\pi}{\Lambda}\right)B + \kappa_{ba}A \quad (4.9)$$

It is apparent from (4.8-9) that the aforementioned frequency at which total reflection can occur is $\beta=\pi/\Lambda$ (Note $\beta-2\pi/\Lambda=-\beta$). (4.8-9) are normally expressed as:

$$\frac{dA}{dz} = -j\delta A + j\kappa B \quad (4.10)$$

$$\frac{dB}{dz} = -j\kappa A + j\delta B \quad (4.11)$$

where δ is the detuning parameter

$$\delta = \beta - \frac{\pi}{\Lambda} \quad (4.12)$$

By expanding β around the frequency ω_b for which $\beta(\omega_b)=\pi/\Lambda$, the detuning parameter is found to be:

$$\beta = \beta(\omega_o) + \frac{d\beta}{d\omega}(\omega - \omega_o) \Rightarrow \delta = \frac{\omega - \omega_o}{v_g} \quad (4.13)$$

where v_g is the group velocity, $d\omega/d\beta$. The propagation constant is found from the eigenvalues of the coupling equations

$$\gamma = \pm\sqrt{\kappa^2 - \delta^2} \quad (4.14)$$

and the eigenfunctions are:

$$A = A_+ e^{\gamma z} + A_- e^{-\gamma z} = A_+ e^{j\beta z} + A_- e^{-j\beta z} \quad (4.15)$$

$$B = B_+ e^{\gamma z} + B_- e^{-\gamma z} = B_+ e^{j\beta z} + B_- e^{-j\beta z} \quad (4.16)$$

Thus the propagation constants are:

$$\beta = \pm\sqrt{\delta^2 - \kappa^2} \quad (4.17)$$

If δ^2 is less than κ^2 , then β is imaginary, implying reflection. As the frequency approaches the Bragg frequency, ω_b , δ becomes smaller, and more of the field is reflected. This part of the spectrum is the stop band of the DFB.

Only two of the constants in eq. (4.15-16) are independent since using eq (4.10-11) B_+ and B_- can be expressed in terms of A_+ and A_- :

$$B_+ = \frac{\beta + \delta}{\kappa} A_+ \quad B_- = \frac{-\beta + \delta}{\kappa} A_- \quad (4.18)$$

4.3 Dispersion

The DFB will be used to compensate for the chirp in the pulse due to nonlinearities in the diode. In order to satisfy the mode-locking equations, the DFB will be designed to have a certain amount of dispersion for a given length. The dispersion parameter, the second derivative of the propagation constant, is given by:

$$\beta'' = \frac{\kappa^2}{v_g^2 \sqrt{\delta^2 - \kappa^2}^3} \quad (4.19)$$

It is desirable that the DFB is parabolic over the bandwidth of the pulse so that third order dispersion is negligible and the propagation constant is second order only in frequency. Third order dispersion is given by:

$$\beta''' = \frac{3\delta\kappa^2}{v_g^3 \sqrt{\delta^2 - \kappa^2}^5} \quad (4.20)$$

Third and higher order parameters can be ignored if the following inequality holds over the bandwidth of the pulse

$$\frac{2\pi \beta'''}{\tau 3\beta''} = \frac{2\pi\delta}{\tau v_g (\delta^2 - \kappa^2)} \ll 1 \quad (4.21)$$

where τ is the pulsewidth at half maximum. The above ratio decreases with increasing pulse width. Increasing κ will also indirectly decrease the ratio because to obtain a certain dispersion with a higher coupling coefficient δ must also be increased. However, increasing κ or τ is undesirable. The object is to produce as short a pulse as possible, and it is difficult to fabricate a DFB with a very high coupling coefficient. **Figures 4.2 and 4.3** graph second- and third-order dispersion versus δ . **Figure 4.4** graphs the ratio of eq (4.21) for different pulsewidths.

Note that δ can be a positive or negative quantity depending on which side of the stop band is being used. One should also realize that the propagation constant can be positive or negative and so can the group velocity and dispersion parameter. Since the model is only concerned with forward waves, a positive group velocity is needed for whatever dispersion is

necessary. Figure 4.5 graphs the propagation constant versus δ and Table 4.1 below lists the sign of δ , β , $\beta'=1/v_g$, and β'' for each quadrant. Once the theoretical analysis is completed, the dispersion needed will be known, and Table 4.1 will be useful in figuring out the right parameters to use.

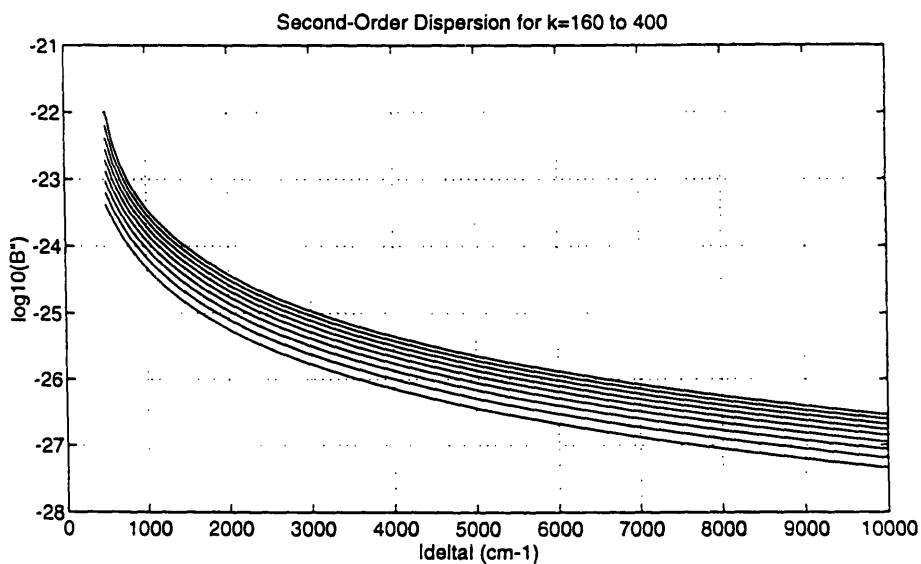


Figure 4.2. Second-order dispersion versus $|\delta|$ for $\kappa=160$ to 400cm^{-1} .

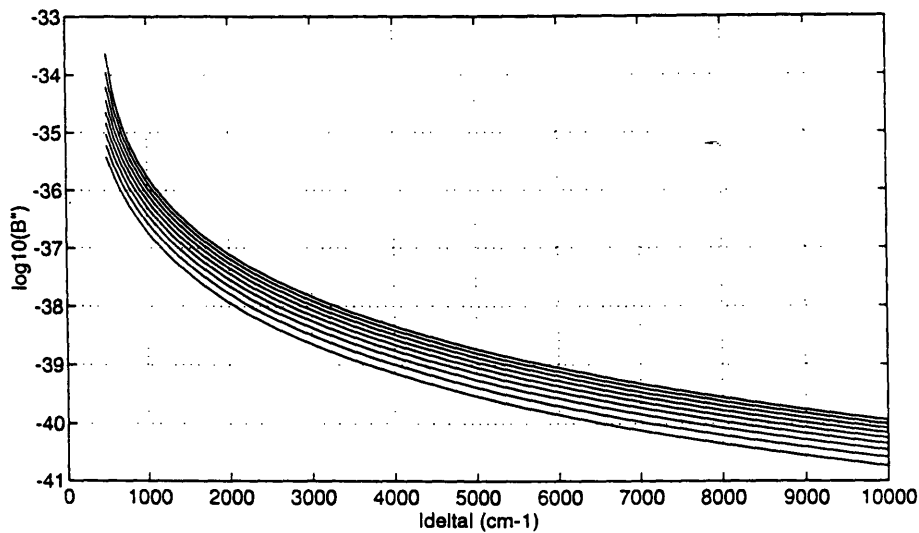


Figure 4.3. Third-order dispersion versus $|\delta|$ for $\kappa=160$ to 400cm^{-1} .

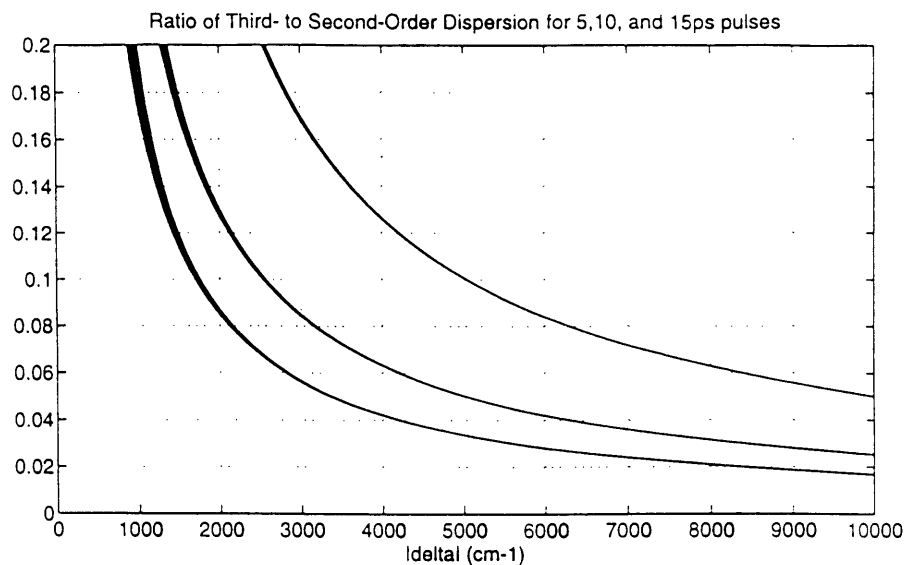


Figure 4.4. Ratio of third- to second-order dispersion for 5, 10, and 15ps pulses.

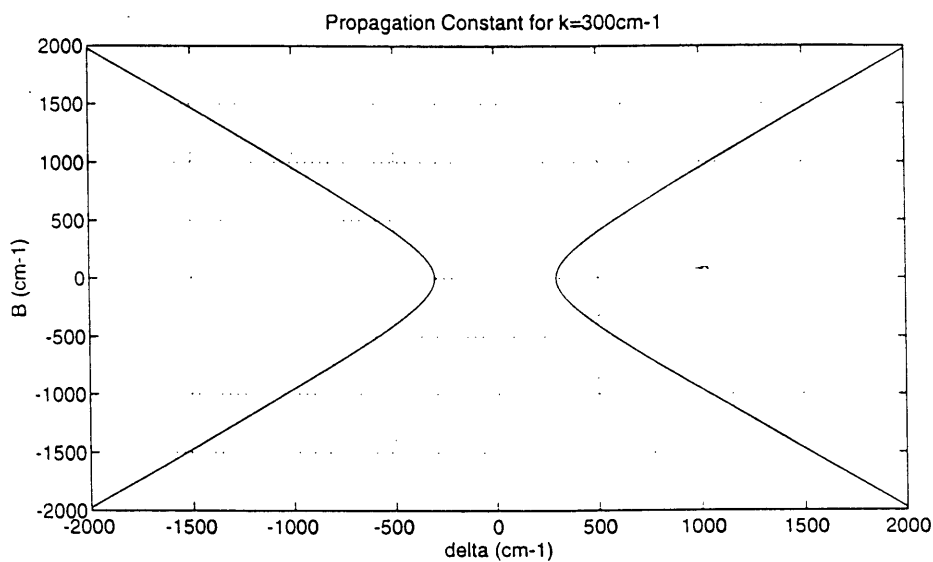


Figure 4.5. Plot of both positive and negative propagation constants, β , versus δ . The area in the middle is the stop band where β is imaginary.

Table 4.1. Signs of propagation parameters in the four quadrants as referred to in Figure 4.5.

	I	II	III	IV
δ	-	+	-	+
β	+	+	-	-
β'	-	+	+	-
β''	-	-	+	+

4.4 Matching Structure

In this ring model, the wave should propagate in only one direction. There will be reflections from the DFB traveling in the opposite direction and because this model has an isolator on one side of the diode, the energy in these waves will be lost. Furthermore, the reflected waves that travel through the diode will deplete the carrier density of the diode and decrease the gain. Therefore, it would be helpful to add a structure on each end of the DFB structure to match the grating to the diode and thus decrease the reflection coefficient seen by the wave when first entering the DFB structure.

The reflection coefficient is $\Gamma=A/B$ can be expressed as a function of position, z , in terms of the reflection coefficient at $z=0$, $\Gamma_0=\Gamma(z=0)$, using the coupling equations (4.10-11):

$$\Gamma = \frac{-j \sin \beta z + \frac{\beta}{\kappa} \Gamma_0 \cos \beta z + j \frac{\delta}{\kappa} \sin \beta z}{\frac{\beta}{\kappa} \cos \beta z - j \frac{\delta}{\kappa} \sin \beta z + j \Gamma_0 \sin \beta z} \quad (4.22)$$

where β is the propagation constant of the DFB as in eq (4.17).

Figure 4.6 shows the entire structure where the middle grating is for chirp compensation and the grating and gaps on either side is for matching purposes. The initial assumption in the analysis of this structure is that the reflection coefficient at $z=0$ is zero. As shown by Haus [6], the reflection coefficient as a function of distance can be described by the Smith chart, Figure 4.7.

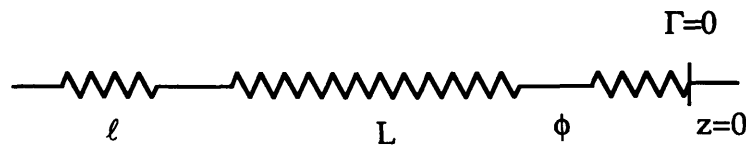


Figure 4.6. Matching structure.

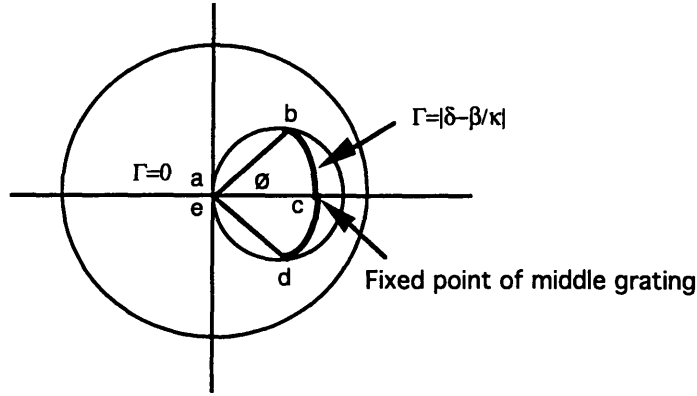


Figure 4.7. Smith chart model following Γ of the matched DFB structure.

Beginning at $z=0$, the reflection coefficient is zero, represented by the origin of the chart (a). Traveling away from $z=0$ in the negative direction, the reflection coefficient follows a circle as shown in the figure until the end of the first section of grating(b). In the gap between the first and middle gratings, the reflection coefficient follows a circle concentric to the origin since the gap simply provides a phase shift dependent on its length. The length of the first grating and the gap should be such that the reflection coefficient at the end of the gap matches that of the middle grating when driven by its eigensolutions. This reflection coefficient from (4.10-11) is simply:

$$\Gamma = \frac{\delta - \beta}{\kappa} \quad (4.23)$$

When driven by the eigensolution, the reflection coefficient of the middle grating remains constant throughout the grating(c).

Another gap of the same length after the middle grating shifts the coefficient again onto the circle of the first grating (d). Through the last section of grating the reflection coefficient follows that circle back to the origin as depicted in the figure (e). Thus, both ends of the structure have a reflection coefficient of zero.

The length of the two end gratings and the gaps are determined by the magnitude of the reflection coefficient of the middle grating, In order for matching to occur, the magnitude of Γ at the end of the first grating (and at the beginning of the second grating) must be the same as the middle grating:

$$\Gamma = \left| \frac{\delta - \beta}{\kappa} \right| \quad (4.24)$$

Eq (4.12) can be simplified by setting $\Gamma_0=0$, and the length of the end gratings can be found by setting eq (4.12) equal to eq (4.24):

$$\beta\ell = \sin^{-1} \frac{\frac{\beta \delta_o - \beta}{\kappa} \frac{\kappa}{\kappa}}{\sqrt{1 - \frac{(\delta_o - \beta)^2}{k^2}}} \quad (4.25)$$

The length of the gap is determined by the phase shift required to transform Γ to the that of the middle grating:

$$\Phi_o = \frac{\pi}{2} - \tan^{-1} \left(\frac{\delta_o}{\beta} \tan \beta\ell \right) \quad (4.26)$$

and the length is:

$$\ell_g = \frac{\Phi_o c}{\omega_o n} \quad (4.27)$$

ω_o and δ_o above refer to the values of ω and δ at which a perfect match is obtained.

The matching structure should be designed for the center frequency of the signal, i.e. the carrier frequency of the diode. The bandwidth of this structure will be analyzed once the parameters are set. Hopefully, Γ will be less than .1 over the bandwidth of the pulse (but don't hold your breath).

4.5 Coupling Coefficient

The magnitude of the coupling between the forward and backward wave is expressed by the coupling coefficient, κ . Power conservation dictates that:

$$\kappa_{ab} = \kappa_{ba}^* = j\kappa \quad (4.28)$$

The evaluation of κ for a particular DFB structure is given by Haus [7].

$$\kappa_{ab} = \frac{-j\omega^2 \mu_o k_x (\epsilon_i - \epsilon) h}{4\beta} \frac{\cos^2 k_x d}{k_x d + \frac{1}{2} \sin 2k_x d + \frac{-k_x}{\alpha_x} \cos^2 k_x d} \quad (4.29)$$

κ is shown to depend on the difference in dielectric constants between the inside (ϵ_i) and the outside (ϵ) of the waveguide, and also on the amplitude of the perturbations (h).

It can be seen from (4.29) that κ increases with increasing perturbation amplitude and increasing difference in dielectric constants.

Unfortunately, it becomes increasingly difficult to fabricate a DFB with large perturbation amplitudes and dielectric differences, i.e. a high coupling coefficient. The highest coupling coefficient recorded to date is $\kappa=300\text{cm}^{-1}$, although generally κ tends to be less than 200cm^{-1} .

Earlier a tradeoff was mentioned between pulsewidth and κ in order to be able to neglect third-order dispersion. It would be nice if both could remain small, but rather than make the pulse too wide, κ will be increased beyond realistic bounds. However, very high coupling coefficients are possible with photonic band gaps.

Chapter 5

Simulation Models

5.1 Introduction

A printout of the program can be found in the appendix and has been commented for easy reading. It was written in fortran simply because the author of this thesis was most familiar with it. Most simulations were run on the RLE VM systems.

Following is a description of the algorithms used in simulating the entire cavity. The program was developed in separate parts, the diode and the DFB structure, and later combined to form the entire ring.

5.2 Simulating the Semiconductor Laser

The primary tools used for simulation of the semiconductor laser diode were the rate equations given in section 3.3. (3.2) is used to determine the carrier density, and (3.3) is used to calculate the gain experienced by the field. The units of all the terms have not yet been discussed. P represents photons per volume (eV/m^3), and field strength squared, or intensity, is $\text{eV}/\text{s}=\text{Watts}$. The intensity, $|a|^2$, and photon density are related by:

$$|a|^2 = v_g A_{\text{eff}} P \quad (5.1)$$

where A_{eff} is the effective transverse area of the active region. In order to apply the rate equations, the present carrier and photon densities and current value must be known. The photon density, P , on the right side of the rate equations, is approximated as the incoming photons. The carrier density is given an initial value determined by the dc current, and is recalculated for every point in time using P and I , which is separately calculated for that time.

The differential change in N is added to the current value to find N for the next point:

$$N_2 = \left(\frac{I}{qV} - \frac{N_1}{\tau_e} - g_o(N_1 - N_t)|a_i|^2 / A_{eff} \right) \Delta t + N_1 \quad (5.2)$$

where Δt is the time difference between points. In an effort to reduce error, the fourth-order Runge-Kutta method [8] was used to calculate the differential change in N.

The change in photon density is proportional to the difference between the intensity of the field going into the diode and the intensity of the field coming out, where intensity is the square of the field strength. Eq. (5.2) shows that increasing intensity increases the photon density in the diode and thus the intensity of the field exiting the diode. This is because more photons entering the diode cause more stimulated emission and therefore more photons to leave the diode. Finally the relation between the field strength and the differential change in photon density is:

$$V \frac{dP}{dt} = |a_o|^2 - |a_i|^2 \quad (5.3)$$

where a_o is the field coming out of the diode, a_i is the field going in, and V is the volume of the diode. The intensity leaving the diode is:

$$|a_o|^2 = \left(-\frac{P}{\tau_p} + g_o v_g \Gamma(N - N_t) P \right) \ell A_{eff} + |a_i|^2 \quad (5.4)$$

$$= \left[\left(-\frac{1}{v_g \tau_p} + g_o \Gamma(N - N_t) \right) \ell + 1 \right] |a_i|^2 \quad (5.5)$$

If (5.5) were to be expressed in exponential terms, it would be:

$$|a_o|^2 = |a_i|^2 \exp \left(-\frac{\ell}{v_g \tau_p} + g_o \ell \Gamma(N - N_t) \right) \quad (5.6)$$

This shows that the simulation fits in very well with the mode-locking theory.

The above equations only work if the changes are very small, meaning that the diode is very short, especially because the shape of the pulse could change within the diode. The entire diode is too long, so it is divided up into sections. The carrier density is calculated separately for each section although they all start with the same initial value.

So far, only the change in amplitude has been determined, but due to propagation through the diode and its nonlinear effects, the phase is greatly changed as well. Assuming that each section is short enough, propagation

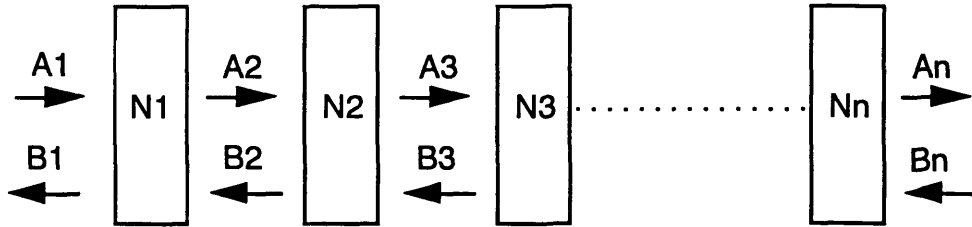


Figure 5.1. Model of diode used for simulations. The diode is divided into sections, each with an independent carrier density, and has field arrays in between.

and nonlinearity is applied separately from the gain, thus at this point the signal has the same phase as it did going into the diode. This intermediate pulse (old phase, new amplitude) is transformed, propagated and transformed again. After propagation, the time dependent nonlinearity is applied, so it is important that the carrier density throughout the pulse is recorded.

The most difficult part of simulating the diode was to find a way to propagate both forward and backward waves through the diode. The solution was to take the forward and backward fields through each section of diode impulse by impulse. This means that the time it takes to travel through each section has to be the same as the time difference between impulses. Between each section, there is an array to which the output of the previous section is added. There are separate arrays for the forward and backward waves (**Figure 5.1**). The intensities of the forward and backward fields are added when calculating the differential change in carrier density, but separate when determining the gain for the two fields. This is correct because the stimulated emissions are emitted in the same direction as the original photon and there is no coupling. Propagation and gain are almost linear functions for a short diode which allows the effects to be additive, but the nonlinearity factor is not. The nonlinearity is applied separately to each impulse before it enters the next section, where the nonlinearity corresponds to the previous section. Thus the error in simulating the diode is minimized.

The DFB structure is actually not expected to produce significant reflections using the matching structure. However, if the bandwidth of the pulse exceeds that of the matching structure or if the ring model is changed to a cavity model, then this program is prepared propagate both directions.

The final effect of the diode is the bandlimiting factor. To include this, the pulse was filtered outside of the diode. The filter is lorentzian, and the bandwidth is on the order of terrahertz.

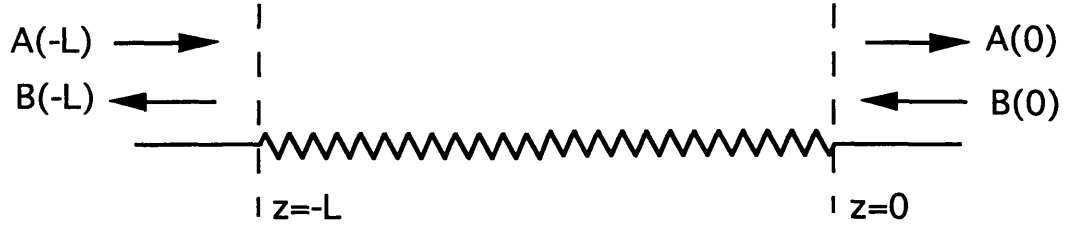


Figure 5.2. Modeling the DFB as a two-port system.

5.3 Modeling the DFB

For simulation purposes, the DFB is modeled as a two-port system. [9] Each port has a forward and backward wave defined at reference planes placed at the ends of the DFB structure. (Figure 5.2) A transfer matrix would describe the relation between the two ports. Along with two boundary conditions, all four waves will be defined uniquely.

The linear differential equations of the DFB coupling the forward and backward waves can be written in matrix form:

$$\frac{d}{dz} X(z) = HX(z) \quad (5.7)$$

H is a square matrix describing the spatial differential changes in the forward and backward waves including their interdependence. $X(z)$ is a column of all the wave amplitudes at the position z . For the DFB structure, (5.7) becomes:

$$\frac{d}{dz} \begin{bmatrix} A(z) \\ B(z) \end{bmatrix} = \begin{bmatrix} -j\delta & j\kappa \\ -j\kappa & j\delta \end{bmatrix} \begin{bmatrix} A(z) \\ B(z) \end{bmatrix} \quad (5.8)$$

Going back to linear algebra, the solution to (5.7) is:

$$X(z) = VE(z)a \quad (5.9)$$

where the columns of V are made up of the eigenvectors of H and $E(z)$ is a square matrix where the diagonals are $\exp(\gamma_n z)$, γ being the eigenvalues of H . a is an arbitrary vector. The eigenvalues are found by satisfying the equation:

$$|H - I\gamma_n| = 0 \quad (5.10)$$

A 2x2 matrix will have two eigenvalues and eigenvectors. The eigenvectors are found from:

$$[H - I\gamma_n]V_n = 0 \quad (5.11)$$

To model the two-port system we need to find a relation between the wave amplitudes at different positions. At the reference planes on the ends of the DFB at $z=0$ and $z=-L$, we know:

$$X(-L) = VE(-L)a \quad \text{and} \quad X(0) = VE(0)a \quad (5.12)$$

Solving for a and substituting gives an equation relating the set of wave amplitudes at two positions.

$$X(-L) = VE(-L)E(0)^{-1}V^{-1}X(0) \quad (5.13)$$

Thus the transfer matrix between the two ports is:

$$T(-L,0) = VE(-L)E(0)^{-1}V^{-1} \quad (5.14)$$

Conversely,

$$X(0) = VE(0)E(-L)^{-1}V^{-1}X(-L) = T(0,-L)X(-L) \quad (5.15)$$

For the DFB structure, the eigenvalues and eigenvectors are:

$$\lambda_{1,2} = \pm\sqrt{\kappa^2 - \delta^2} \quad , \quad V_{1,2} = \frac{\kappa}{j2|\gamma|} \begin{bmatrix} \delta \mp j|\gamma|/\kappa \\ 1 \end{bmatrix} \quad (5.16)$$

Finally, the transfer matrix for a DFB structure of length L is:

$$X(-L) = \begin{bmatrix} \cosh \gamma L + j\frac{\delta}{\kappa} \sinh \gamma L & -j\frac{\kappa}{\gamma} \sinh \gamma L \\ j\frac{\kappa}{\gamma} \sinh \gamma L & \cosh \gamma L - j\frac{\delta}{\kappa} \sinh \gamma L \end{bmatrix} X(0) \quad (5.17)$$

Now, given the forward and backward wave at one port, it is easy to calculate the forward and backward wave at the other port.

Unfortunately, in this simulation the two known waves are the inputs to the DFB structure, meaning the forward wave of the front port and the backward wave of the end port. Thus a scattering matrix would be more appropriate than a transfer matrix, however the elements of the transfer matrix are easily manipulated to form a scattering matrix:

$$T = \begin{bmatrix} T_{11} & T_{12} \\ T_{21} & T_{22} \end{bmatrix} \Rightarrow S = \begin{bmatrix} \frac{T_{21}}{T_{11}} & T_{22} - \frac{T_{21}T_{12}}{T_{11}} \\ 1 & -\frac{T_{12}}{T_{11}} \end{bmatrix} \quad (5.18)$$

Because there is also an isolator at the end of the DFB in this model, the input from the end port is assumed to be zero. The input at the front port is the output of the diode. From these boundary conditions, the reflected and output waves from the DFB are calculated.

For simulating the matching structure, we resort back to the transfer matrix. Each section of grating is represented by its own transfer matrix determined by its length. The gaps also have a transfer matrix:

$$G(\ell_g) = \begin{bmatrix} e^{j\frac{n_g}{c}\ell_g} & 0 \\ 0 & e^{-j\frac{n_g}{c}\ell_g} \end{bmatrix} \quad (5.19)$$

These matrices are multiplied together to form one transfer matrix describing

$$T_m = T(-l,0)G(l_g)T(-L,0)G(l_g)T(-l,0) \quad (5.20)$$

the entire matching structure. This final transfer matrix is transformed into a scattering matrix to be used in the simulations.

5.4 Combination Design

The DFB structure takes input from one side and produces output on both sides since part of the field is reflected and most travels through. There is no input from the other side because an isolator is modeled on the other side of the diode. The output of the final section of the diode is the input of the DFB. Once again this is done impulse by impulse. The reflection from the DFB is added to the backward field array for the last section of diode, and what goes through is added to the forward field array of the first section of the diode. The DFB is also a linear structure, thus it is perfectly legal to add the results of each impulse.

Before the field enters the diode through the first section, the loss is applied to the field. The loss is constant over time and frequency and is calculated to be a fraction of the gain since there cannot be more loss than gain.

In order to start the mode-locking process, a gaussian pulse is fed into the first forward array. It was attempted to synchronize the peak of the pulse and the peak of the carrier density in the hope that the laser would reach steady state faster. However, it is not necessary because the pulse will move, shrink, and shift in frequency as all the effects within the cavity dictate. It only needs some introduction of photons and enough time to reach steady state. Time was actually a problem--the program takes a very long time to run because of all the arrays. To run tests, the diode was shortened, and gain was doubled to compensate.

Chapter 6

Mathematical Analysis

6.1 Introduction

Before running simulations, it is helpful to perform a mathematical analysis of the carrier density in order to predict the results. Once a formula for the carrier density, and therefore the gain, has been established, we can return to the mode-locking equations from chapter 2. Finally, the unknowns that determine the pulse can be defined. More importantly, the amount of dispersion necessary to produce a pulse without chirp can be calculated. This result will determine the parameters of the DFB structure.

Following is first the analysis of the carrier density originating from the rate equations and finishing with gain. Next is an analysis of the mode-locking equations, and solutions for each of the parameters of the pulse are given. In the end, the DFB structure will be designed, and the effect of its dispersion will be described.

6.2 Carrier Density

The rate equation (3.2) describes the carrier density for all time given the current and optical intensity. To simplify the analysis, the equation is separated into two parts: one to express the carrier density as a result of the current, and the second to express the saturation effect from the presence of photons. So,

$$\frac{dN_i}{dt} = \frac{-N_i}{\tau_e} + \frac{I}{qV} \quad \text{and} \quad \frac{dn}{dt} = \frac{-n}{\tau_e} - g_o v_g (N - N_i) P \quad (6.1a,b)$$

and the total carrier density is the sum of the solutions to these two equations: $N=N_i+n$.

Looking at (6.1a) first, the current applied to the diode should be a dc current equivalent to the threshold current given in section 3.2 or below plus a modulated current with the modulation frequency determined by the roundtrip time (ω_m).

$$I = I_{dc} + I_{ac} \cos(\omega_m t + \phi) \quad (6.2)$$

The purpose of the phase shift is so that the peak of the carrier density can be set at the origin. Combining (6.2) and (6.1a) gives:

$$\frac{dN_i}{dt} = \frac{-N_i}{\tau_e} + \frac{-N_d}{\tau_e} + N_a \cos(\omega_m t + \phi) \quad (6.3)$$

where $N_d = \frac{I_{dc} \tau_e}{qV}$ and $N_a = \frac{I_{ac}}{qV}$

The solution to (6.3) is:

$$N_i = N_d + \frac{N_a \tau_e^2}{1 + \tau_e^2 \omega_m^2} \left(\frac{1}{\tau_e} \cos \phi + \omega_m \sin \phi \right) \cos(\omega_m t) \quad (6.4)$$

Because in these simulations, $\omega_m \gg 1/\tau_e$, $\phi = \pi/2$ and (6.4) can be approximated as:

$$N_i = N_d + \frac{N_a}{\omega_m} \cos(\omega_m t) \quad (6.5)$$

Approximating the saturation effect is a bit more complicated mostly because the time dependence of the photon density is gaussian. Only a second order solution is wanted, therefore the carrier density in the gain term of (6.1b) is set at the peak carrier density found from (6.5). The photon density is proportional to the amplitude of the pulse from the solutions to the mode-locking equations, (2.17).

$$P = |A_p|^2 \exp\left(\frac{-t^2}{\tau^2}\right) \text{ where } A_p \propto A \quad (6.6)$$

so that

$$\frac{dn}{dt} = \frac{-n}{\tau_e} - G(N_{\max} - N_i) |A_p|^2 \exp\left(\frac{-t^2}{\tau^2}\right) \quad (6.7)$$

here $G = g_0 v_g$. Instead of finding a general solution, which is actually impossible, n is expanded into a Taylor series around $t=0$, and the coefficients up to second order are found:

$$n = n_0 + \frac{dn}{dt} t + \frac{1}{2} \frac{d^2 n}{dt^2} t^2 \quad (6.8)$$

The most difficult part is finding n_0 :

$$\begin{aligned}
n_0 &= e^{-\frac{1}{\tau_e}} \int_{-\infty}^t -G(N_{\max} - N_t) |A_p|^2 \exp\left(\frac{-t'^2}{\tau_e^2}\right) dt' \Big|_{t=0} \\
&= -G(N_{\max} - N_t) |A_p|^2 \tau \sqrt{\pi/2} \exp\left(\frac{\tau^2}{2\tau_e^2}\right) (1 - \Phi\left(\frac{\tau}{\sqrt{2}\tau_e}\right)) \\
&\approx -G(N_{\max} - N_t) |A_p|^2 \tau \sqrt{\pi/2}
\end{aligned} \tag{6.9}$$

Now, it is easier to find the other two coefficients:

$$\frac{dn}{dt} \Big|_{t=0} = \frac{-n_0}{\tau_e} - G(N_{\max} - N_t) |A_p|^2 \tag{6.10}$$

$$\frac{d^2n}{dt^2} \Big|_{t=0} = \frac{n_0}{\tau_e^2} - \frac{G}{\tau_e} (N_{\max} - N_t) |A_p|^2 \tag{6.11}$$

Finally the total carrier density is:

$$N = N_d + \frac{N_a}{\omega_m} \cos(\omega_m t) + n_0 + \left(\frac{-n_0}{\tau_e} - G(N_{\max} - N_t) |A_p|^2\right) t + \left(\frac{n_0}{\tau_e^2} - \frac{G}{\tau_e} (N_{\max} - N_t) |A_p|^2\right) \frac{t^2}{2} \tag{6.12}$$

Now that the carrier density has been estimated, the mode-locking equations can be completed.

6.3 Mode-Locking

In section 2.3, the master equation was formulated, but it was in a rather general form. Using the solutions for the carrier density, some of the variables in (2.16) can be further defined. The first to be considered is the gain and saturation terms, $G(t)$ and $S(t)$.

To find gain in the diode, the solutions to the carrier density above are substituted into to the photon rate equation (3.3). Because the dc current is set at threshold, the dc carrier density, N_d , exceeds the transparency threshold just enough to cancel the effects of photon decay. So, the total effect of the diode on the amplitude of the pulse is found to be:

$$G(t) - S(t) = \frac{1}{2} \frac{\ell_d}{v_g} (g_0 v_g \Gamma(N_d + \frac{N_a}{\omega_m} \cos(\omega_m t) + n - N_t) - \frac{1}{\tau_p}) = \frac{1}{2} \ell_d g_0 \Gamma\left(\frac{N_a}{\omega_m} \cos(\omega_m t) + n\right) \tag{6.13}$$

The rate equation was applied to photon density or intensity which is proportional to the square of the actual amplitude of the signal. Because the gain is modelled as an exponential effect, taking the square root to apply the gain to the signal means taking half the argument, thus the one-half term at the beginning of the left side of (6.13). The other terms at the beginning can

be traced from Chapter 5 in the conversion from the signal to intensity (section 5.2).

Separately, the gain and saturation terms are:

$$G(t) = \frac{1}{2} \ell_d g_o \Gamma \left(\frac{N_a}{\omega_m} \cos(\omega_m t) \right) \quad (6.14)$$

$$S(t) = -\frac{1}{2} \ell_d g_o \Gamma n = -\frac{1}{2} \ell_d g_o \left(n_o + \frac{dn}{dt} t + \frac{1}{2} \frac{d^2 n}{dt^2} t^2 \right) \quad (6.15)$$

In order to simplify further equations, saturation is expressed as:

$$S(t) = S_1 + S_2 t + S_3 t^2$$

Note that $S_{1,2,3}$ are dependent on the amplitude and width of the pulse. Since the focus is on a single pulse centered at the origin, (6.14) can be approximated as [10]:

$$G(t) = \frac{1}{2} \ell_d g_o \Gamma \frac{N_a}{\omega_m} (1 - \omega_m^2 t^2) = G(1 - \omega_m^2 t^2) \quad (6.16)$$

here G is the product of the first terms at the beginning of the middle of (6.16) and shall remain so for the rest of the thesis.

One discrepancy between the simulations and the model of Chapter 2 is the bandlimiting of the gain medium. The simulations filter the pulse outside the diode, so instead of g_o/ω_g^2 is just $1/\omega_g^2$.

The rewritten version of the master equation using all of the new found terms is:

$$\begin{aligned} & \left[G(1 - \omega_m^2 t^2) - (S_1 + S_2 t + S_3 t^2) \right] (1 + j\alpha) - L + jD_d \frac{d^2}{dt^2} + jD_p \frac{d^2}{dt^2} + \frac{1}{\omega_g^2} \frac{d^2}{dt^2} \\ & = j\psi + \delta T \frac{d}{dt} \end{aligned} \quad (6.17)$$

Once again, the shape of the pulse is proposed to be:

$$a = A \exp\left(-\frac{t^2}{2\tau^2} (1 + j\beta)\right) \exp(-j\Delta\omega t) \quad (6.18a)$$

and from this:

$$\frac{da}{dt} = \left[\frac{-(1 + j\beta)t}{\tau^2} - j\Delta\omega \right] a \quad (6.18b)$$

$$\frac{d^2 a}{dt^2} = \left[-\frac{1}{\tau^2} - \Delta\omega^2 - \frac{j\beta}{\tau^2} + \frac{j2\Delta\omega t}{\tau^2} - \frac{2\Delta\omega\beta t}{\tau^2} + \frac{(1 - \beta^2)t^2}{\tau^4} + \frac{j2\beta t^2}{\tau^4} \right] a \quad (6.18c)$$

Substituting (6.18b,c) into (6.17) and separating the imaginary and real terms and the constant, linear, and quadratic (in time) terms, gives six equations.

The six unknowns are $|A|$, τ , β (chirp parameter), $\Delta\omega$ (frequency shift), ψ (phase shift), and δT (time shift from the origin).

The six equations are:

Constant Terms

$$\text{Real:} \quad G - S_1 - L + D_d \frac{\beta}{\tau^2} + D_{fb} \frac{\beta}{\tau^2} + \frac{-1}{\omega_g^2} \left(\frac{1}{\tau^2} + \Delta\omega^2 \right) = 0 \quad (6.19a)$$

$$\text{Imaginary:} \quad \alpha G - \alpha S_1 - (D_d + D_{fb}) \left(\frac{1}{\tau^2} + \Delta\omega^2 \right) - \frac{1}{\omega_g^2} \frac{\beta}{\tau^2} = \psi - \delta T \Delta\omega \quad (6.19b)$$

Linear Terms

$$\text{Real:} \quad -S_2 - \frac{2\Delta\omega}{\tau^2} (D_d + D_{fb}) - \frac{1}{\omega_g^2} \frac{2\Delta\omega\beta}{\tau^2} = -\delta T \frac{1}{\tau^2} \quad (6.19c)$$

$$\text{Imaginary:} \quad -\alpha S_2 - \frac{2\Delta\omega\beta}{\tau^2} (D_d + D_{fb}) + \frac{1}{\omega_g^2} \frac{2\Delta\omega}{\tau^2} = -\delta T \frac{\beta}{\tau^2} \quad (6.19d)$$

Quadratic Terms

$$\text{Real:} \quad -G\omega_m^2 - S_3 - \frac{2\beta}{\tau^4} (D_d + D_{fb}) + \frac{1}{\omega_g^2} \frac{(1-\beta^2)}{\tau^4} = 0 \quad (6.19e)$$

$$\text{Imaginary:} \quad -\alpha G\omega_m^2 - \alpha S_3 + \frac{(1-\beta^2)}{\tau^4} (D_d + D_{fb}) + \frac{1}{\omega_g^2} \frac{2\beta}{\tau^4} = 0 \quad (6.19f)$$

Eq. (6.19a-f) can be manipulated to find solutions for the parameters of the pulse shape. Most important is to find β , the chirp parameter, and τ which defines the pulse width. Combining (6.19e) and (6.19f) will give the solutions to β and τ providing that S_3 is neglected. After some preliminary estimates, it was decided that S_3 is insignificant compared to $G\omega_m^2$. β is determined by:

$$\left(\frac{\alpha}{\omega_g^2} - (D_d + D_{fb}) \right) \beta^2 + \left(2\alpha(D_d + D_{fb}) + \frac{2}{\omega_g^2} \right) \beta + (D_d + D_{fb}) - \frac{\alpha}{\omega_g^2} = 0 \quad (6.20)$$

and once β is known τ can be found from:

$$\tau^4 = \frac{\frac{1}{\omega_g^2} - \frac{\beta^2}{\omega_g^2} - 2(D_d + D_{fb})\beta}{G\omega_m^2} \quad (6.21)$$

The objective is to find a value for D_{fb} such that β is zero, ie no chirp. If β is zero, then (6.20) demands that:

$$D_{fb} = \frac{\alpha}{\omega_g^2} - D_d \quad (6.22)$$

Knowing D_{fb} , the DFB structure can be designed. Before getting into the DFB, however, the rest of the pulse parameters must be solved for. The frequency shift, $\Delta\omega$, is the one of the roots of this equation from combining (6.19a,c,d):

$$\frac{\Delta\omega^2}{\omega_g^2} + \hat{S}_1 \frac{\frac{2}{\omega_g^2}(1-\beta^2)}{\hat{S}_2 \tau^2(\beta-\alpha)} \Delta\omega - G + L - (D_d + D_{fb}) \frac{\beta}{\tau^2} + \frac{1}{\omega_g^2 \tau^2} = 0 \quad (6.23)$$

where $S_{1,2}$ have the amplitude dependence, $|A|^2$, divided out. $\Delta\omega$ must be negative in order for the squared amplitude of the signal to be positive:

$$|A|^2 = \frac{\frac{2}{\omega_g^2}(1-\beta^2)}{\hat{S}_2 \tau^2(\beta-\alpha)} \Delta\omega \quad (6.24)$$

δT can be found from eq (6.19c), and ψ is also solved through (6.19b). Finally, given the specifications of the diode and cavity and the running conditions, the pulse can be fully determined.

6.4 Design of the DFB

Now that the amount of dispersion needed from the DFB structure is known, the DFB can be designed. From Chapter 4:

$$\beta'' = \frac{\kappa^2}{v_g^2 \sqrt{\delta_o^2 - \kappa^2}} = \frac{2D_{fb}}{\ell_{dfb}} \quad (6.25)$$

Apparently, the dispersion parameter must be positive, thus in order to have positive dispersion and positive group velocity, the DFB propagation constant must be in quadrant IV in **Figure 4.5**, meaning that the propagation constant is negative and δ is also negative, so the Bragg frequency is larger than the center frequency. Unfortunately, the dispersion of the DFB is not constant over the band width of the pulse, but in an effort to minimize the error, the dispersion will be set for the center frequency of the pulse, ω_o , which corresponds to δ_o :

$$\delta_o = \frac{\omega_o - \omega_b}{v_g} = -\sqrt{\left(\frac{\kappa^2}{v_g^2 \beta''}\right)^{2/3} + \kappa^2} \quad (6.26)$$

The two parameters that define the DFB structure are ω_b and κ . The method used to find values for these parameters was to choose the coupling coefficient and calculate the Bragg frequency from (6.26):

$$\omega_b = \omega_o - \delta_o v_g \quad (6.27)$$

As mentioned earlier, the coupling coefficient should be chosen so that third-order dispersion is negligible which occurs with increasing κ . Also, a bigger coupling coefficient means δ_o is larger, i.e. the Bragg frequency is farther away from the center frequency. This is a good thing not only because third-order dispersion is larger close to ω_b , but also because the spectrum of the pulse should not include the stop band of the DFB structure centered around ω_b . The Bragg frequency also determines the periodicity of the structure, $\Lambda = \pi v_g / \omega_b$.

The length of the DFB structure was set at 1cm for no particular reason, although it had to be long enough for the roundtrip time to be much longer than the pulse width and so that dispersion would be reasonable.

This concludes designing the DFB structure. In order to see the effect of adjustments in the coupling coefficient and calculate the parameters of the pulse shape, a spreadsheet was used (see Appendix). The spreadsheet also lists the values used for the diode and DFB specifications. A lot of these values are from **Table 3.1**.

Chapter 7

Results of Simulations

7.1 Introduction

Yeah! My program works! As stated before, the simulations of the diode and the DFB structure were developed separately. **Figure 7.1** shows what the output of the gain section looks like after one pass of a forward moving pulse and no backward wave. For different currents, the pulses experience different amounts of gain, or absorption if the current is below the threshold value. **Figure 7.2** shows the output of the DFB structure given the same input as the diode. The reflected field from the DFB is so small compared to the field that travels through, that perhaps it could be ignored as its effect on the diode carrier density is minimal. In the theory of Chapter 6, the saturation from the reflected wave was not considered, and it seems from the figure that this was not a bad approximation.

The values used for the simulations can be found in the *Excel* spreadsheets in the appendix. There is a chart for every simulation which not only has the diode and DFB specifications, but also the calculated parameters of the predicted steady-state pulse.

Initially, it was thought that bandlimiting the diode would not be necessary and that the DFB structure would have a stronger bandlimiting effect anyway. **Figure 7.3** shows the result of omitting this factor from the diode. This only happened after several hundred roundtrips before which the results showed normal mode-locking. Apparently, the lack of bandlimiting in the diode causes instabilities which eventually take effect. Presumably, the pulse becomes shorter as the bandwidth was allowed to spread. Once the bandlimiting was applied, the program could run just as

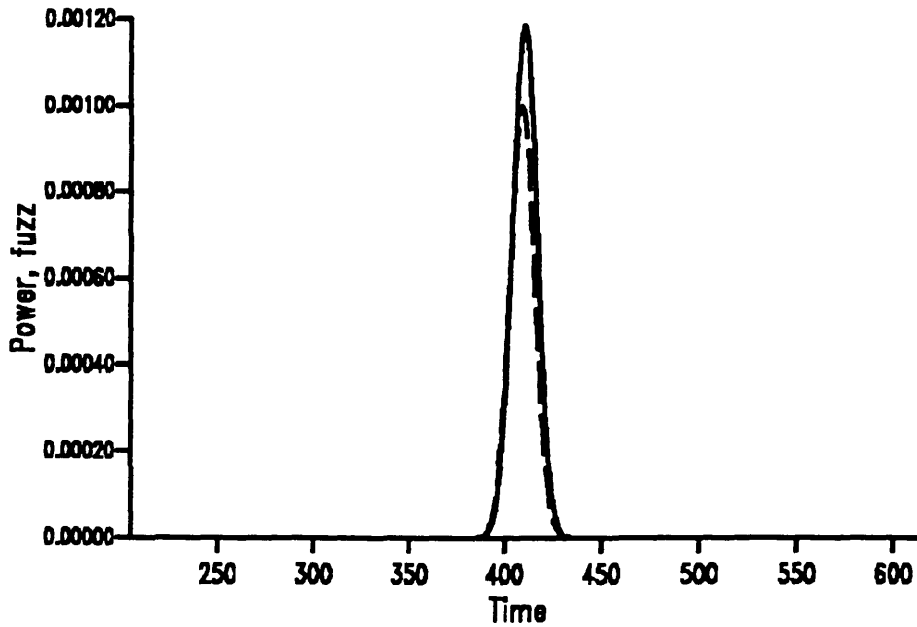


Figure 7.1. Output of the diode. The dashed line is the original pulse, and the solid line is the output with current above threshold.

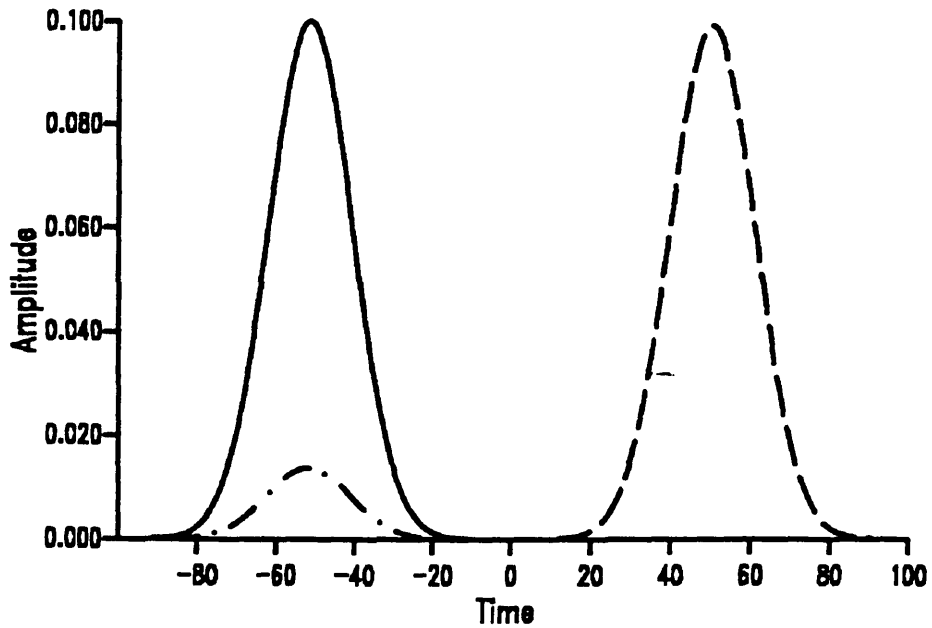


Figure 7.2. Output of the DFB structure: solid line is the input pulse, dashed line is the field that traveled through, and dotted is the reflected field.

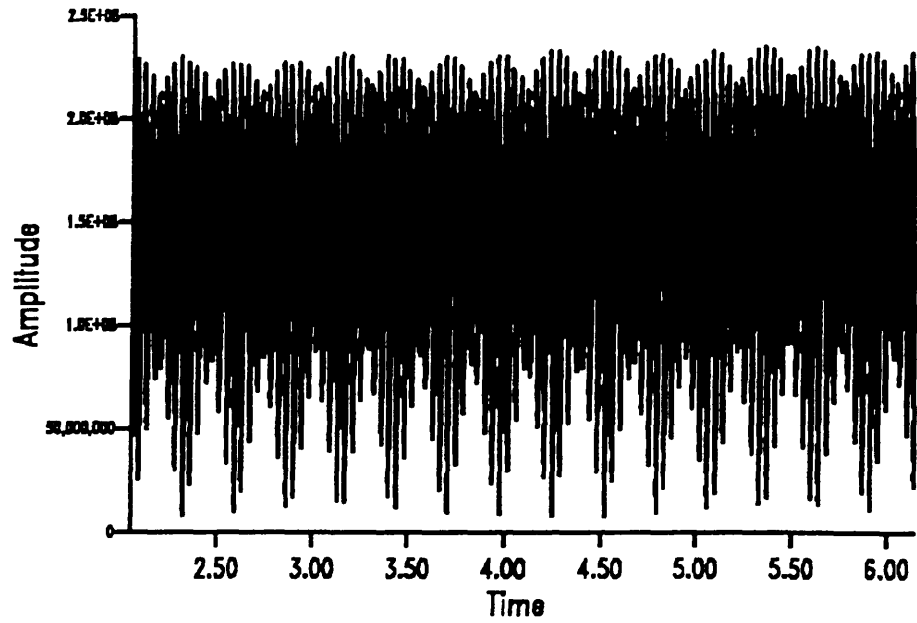


Figure 7.3. Output of simulation with a non-bandlimited diode.

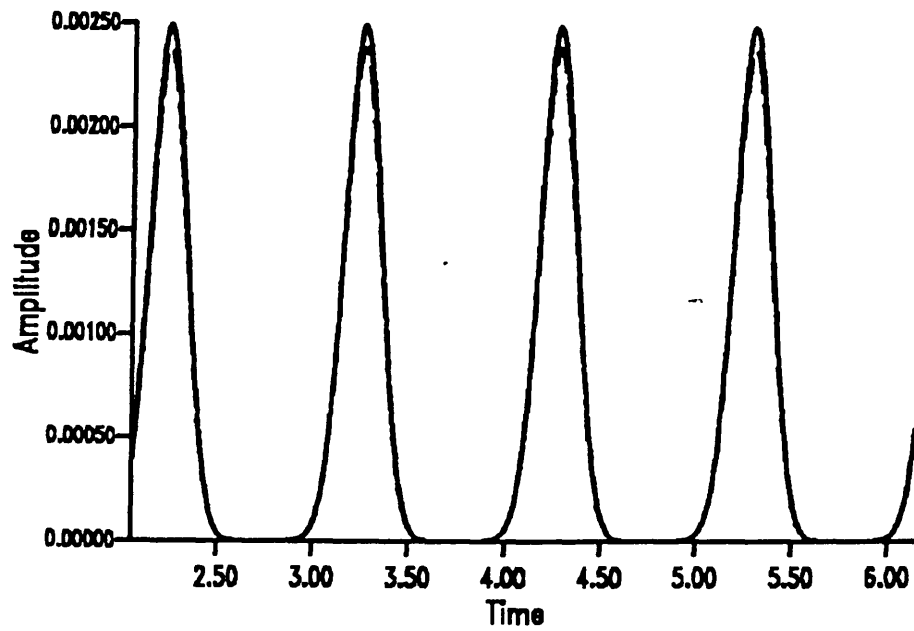


Figure 7.4. Output of simulation with bandlimiting.

long and still produce mode-locked pulses of reasonable width, meaning around 10ps, as **Figure 7.4** shows. This figure is the result of a simulation in which the only change from that of **Figure 7.3** was the application of bandlimiting. The significance of these results is that had the instability not been so obvious it would have been easy to assume that the results without bandlimiting had been correct. Namely, if the simulation produced very short pulses, they would have been happily accepted although it is obvious now that the diode bandlimiting has a strong affect on pulse shaping and to omit it gives erroneous results.

7.2 Testing and Control Simulations

For purposes of comparison, a simulation was run with DFB off, $\kappa=0$, and alpha off, $\alpha=0$. **Figure 7.5** shows the pulse series produced by this simulation, and it is obvious that a steady-state has been reached. The pulsewidth is 7ps. **Figure 7.7** and **7.8** display a single pulse and its phase. The phase is linear during the time of the pulse, meaning that the pulse has no chirp as would be expected with no dispersion and no nonlinearities. Another interesting point about the phase is that there is a phase shift between pulses (not shown in graphs). What happens to the phase between pulses is unaccountable because the intensity should be zero. The frequency spectrum (**Figure 7.6**) has a bandwidth of .0592THz and is still centered at the carrier frequency of the diode. The peak of the pulse occurs simultaneously with the peak of the carrier density.

To insure that the DFB is working and show what its effect is, a simulation was run with the DFB on and alpha off. The coupling coefficient was set 1000cm^{-1} which is much too high and dispersion was negative, but the object was just to demonstrate the effect of the DFB. The results show most notably some double pulsing developing (**Figure 7.9**). The reasons for this will be suggested later. What is important to see is the phase of one roundtrip section of time. The curvature of the phase is a sign of chirp and is a result of the dispersion from the DFB structure (**Figure 7.11**).

To demonstrate the nonlinearity of the diode, a simulation was done with the DFB off and alpha on, $\alpha=5$. **Figure 7.12** shows a series of pulses and where they occur in relation to the carrier density. Again, it is obvious that steady-state has been established. the peak of the pulse and the peak of the

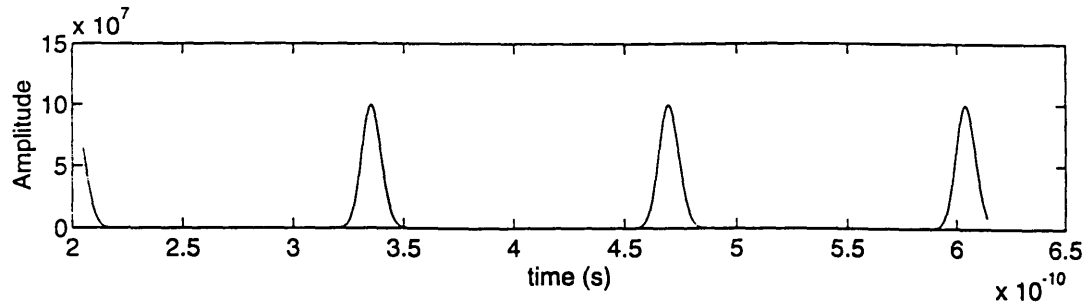


Figure 7.5. Pulse series produced in simulation with both DFB and alpha off.

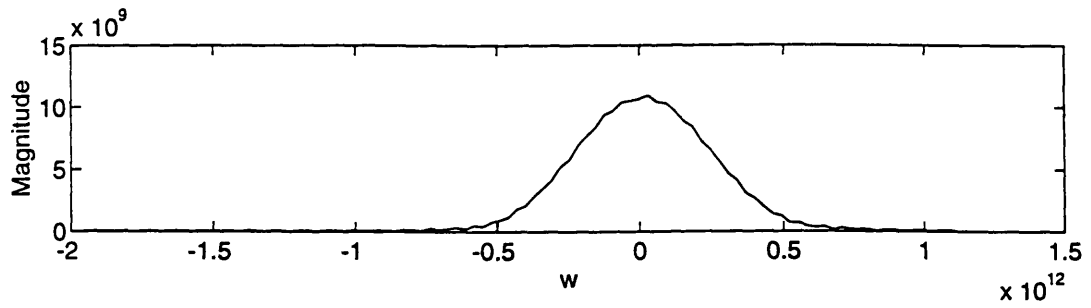


Figure 7.6. Frequency spectrum of a single pulse from the above series.

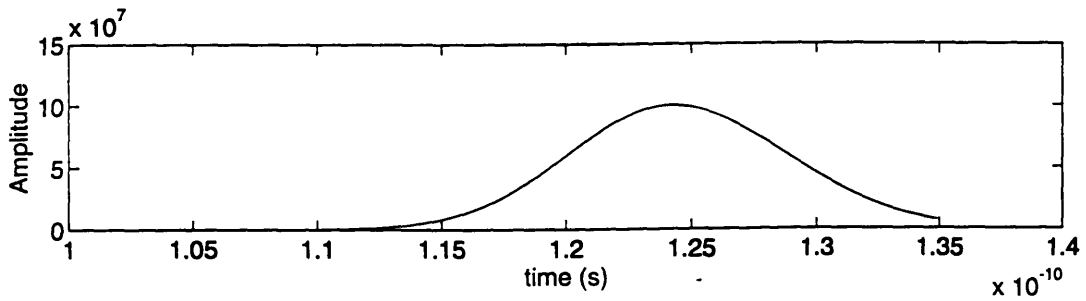


Figure 7.7. A single pulse from the simulation with both DFB and alpha off.

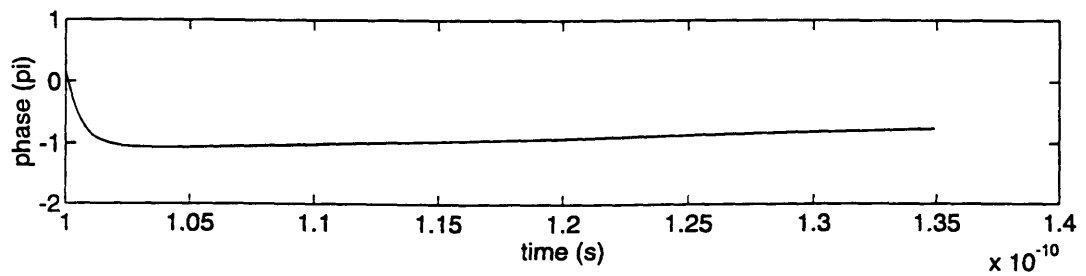


Figure 7.8. Phase of the above pulse.

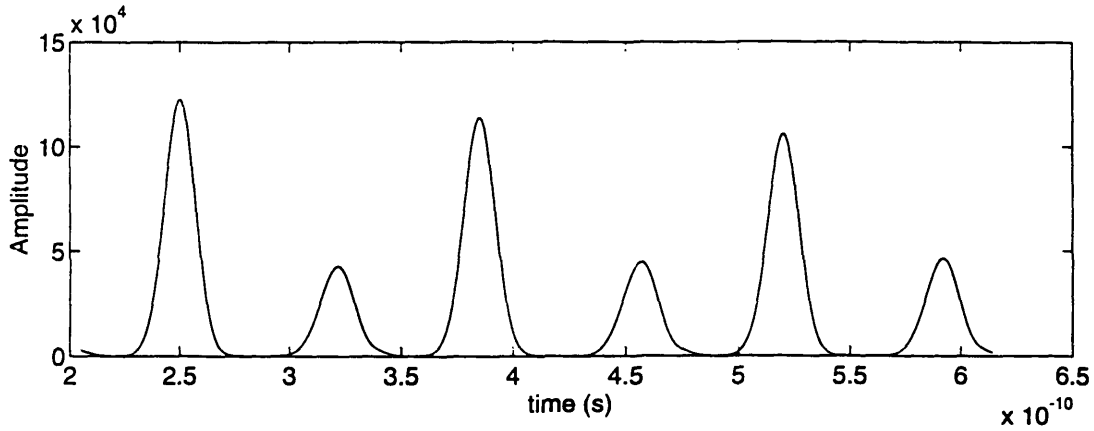


Figure 7.9. Series of pulses from simulation with alpha off and DFB on.

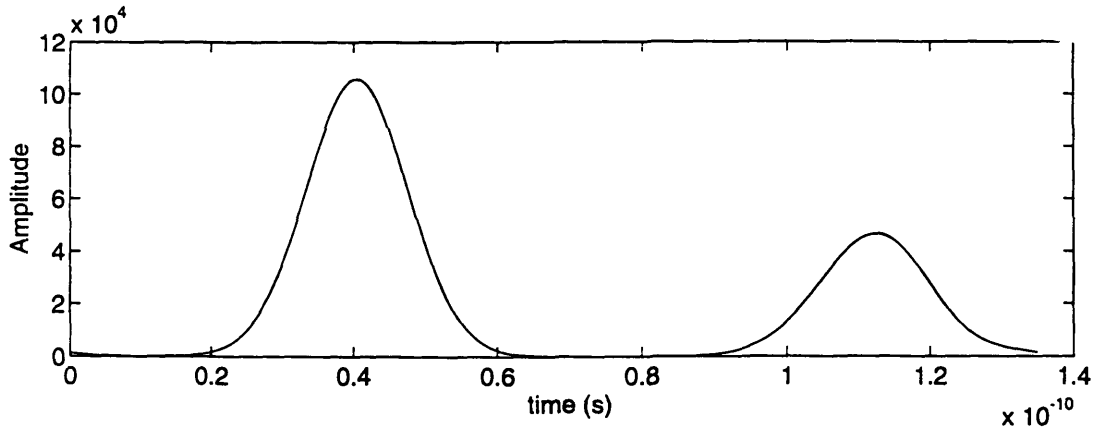


Figure 7.10. Section of above series one roundtrip in length.

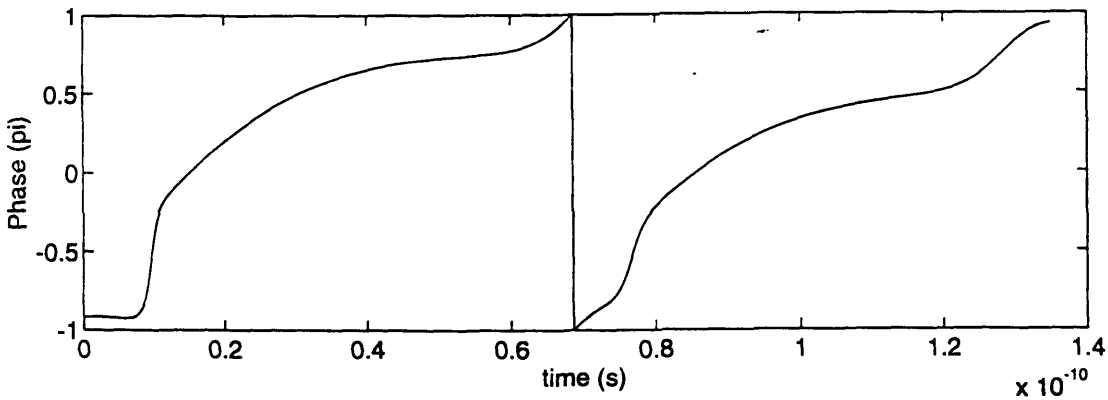


Figure 7.11. Phase corresponding to Figure 7.10.

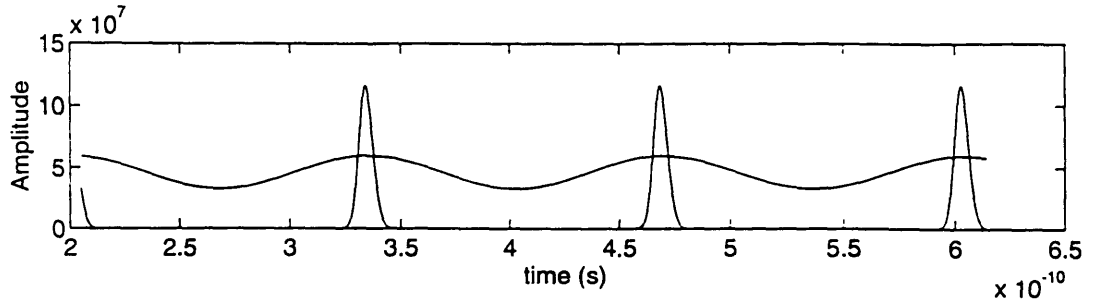


Figure 7.12. Series of pulses from simulation with DFB off and alpha on. Sinusoidal line is relative carrier density (not actual values).

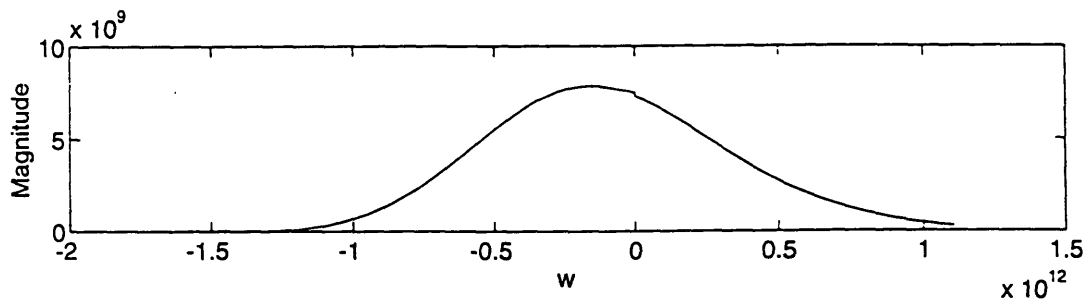


Figure 7.13. Frequency spectrum of a single pulse from the above series.

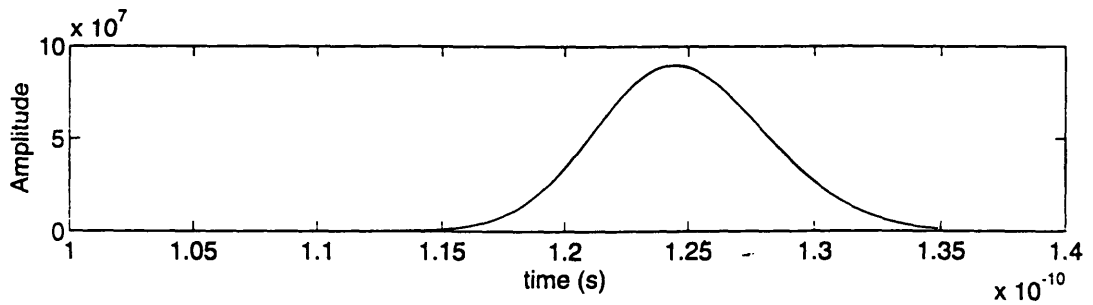


Figure 7.14. Single pulse from simulation with DFB off and alpha on.

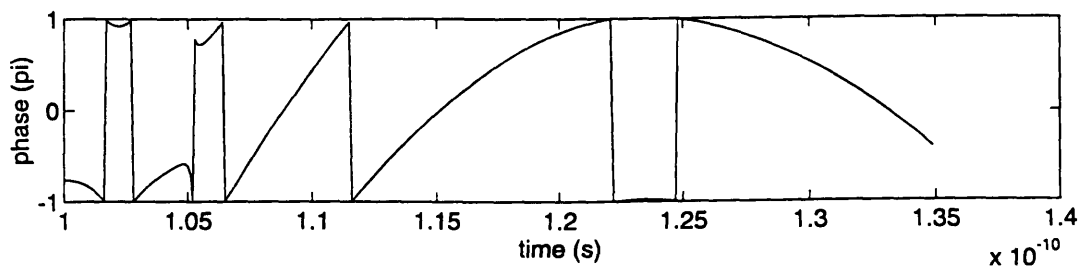


Figure 7.15. Phase corresponding to Figure 7.14.

carrier density seem to coincide, and indeed the δT predicted is very small. The pulse width is 5.2ps and the bandwidth is .0987THz. A slight frequency shift can be seen in **Figure 7.13**, but is not as large as expected. The most informative feature of these pulses is the phase. The phase during the time of the pulse is almost gaussian looking and certainly seems to have quadratic time dependence--a sure sign of chirping due to the nonlinearities of the diode (**Figure 7.15**).

These three tests demonstrate that the program is working properly and gives something to compare the experimental simulations with. Following, are the results of simulations run with the DFB designed for three different amounts of dispersion.

7.3 Results

According to the equations of Chapter 6, the best result was expected for $D_{fb}=1.2662 \times 10^{-25} s^2$ for $\alpha=5$. **Figure 7.16** shows a series of pulses produced by this simulation and the relative carrier density. Unfortunately, there is double pulsing. The main pulse is shifted by 25ps off the peak of the carrier density which may be the cause for the double pulsing as will be explained later. The amplitude of the pulse is far below expectations (see appendix), however, due to the presence of the second pulse. The pulse width of the larger pulse is 20.6ps, and the bandwidth is about .00986THz which is very small but typical of the longer pulse. Looking at **Figure 7.19**, the phase during the pulse is very linear, thus even though it looks horrible at least the chirp was canceled. The phase has a negative slope indicating a frequency shift as is seen from the spectrum of the pulse.

Several different simulations were run to prevent the double pulsing but everything that was done seemed to make it worse. Increasing κ had little or no effect, and increasing the modulation current only made it worse. By accident, simulations were run with less dispersion and gave surprisingly good results.

The next simulation had five times less the dispersion of the above simulation, $D_{fb}=2.53 \times 10^{-26} s^2$. The series of pulses in **Figure 7.20** shows that steady-state has not yet been reached since the larger pulse is growing and the small pulse is shrinking, but at least it promises to look better than the previous simulation. The peak of the larger pulse is not shifted as far from the peak of carrier density and the peak of the small pulse seems to coincide

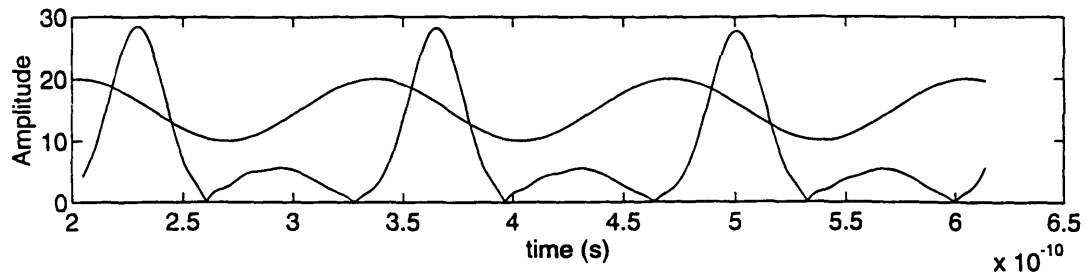


Figure 7.16. Series of pulses from simulation with $D_{fb}=1.2662 \times 10^{-25}$ and $a=5$. Sinusoidal line is relative carrier density (not actual values).

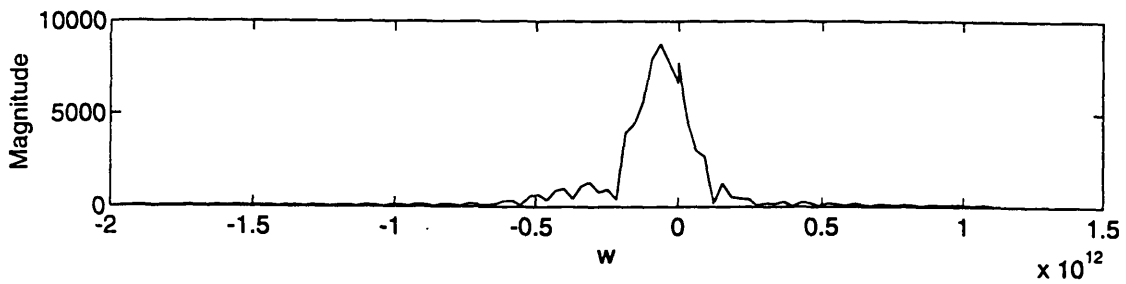


Figure 7.17. Frequency spectrum of a single pulse from the above series.

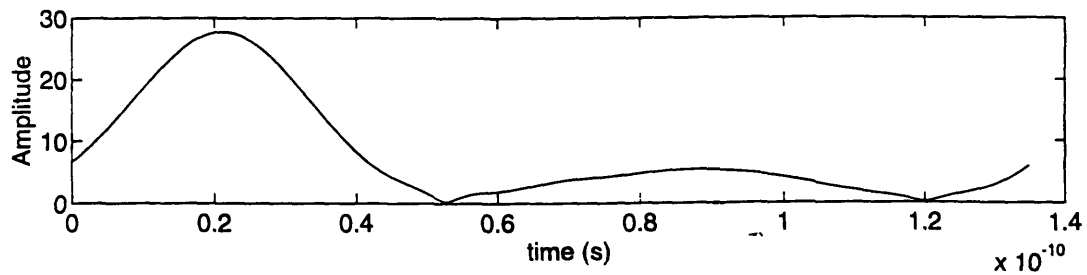


Figure 7.18. Single pulse from simulation with $D_{fb}=1.2662 \times 10^{-25}$ and $a=5$.

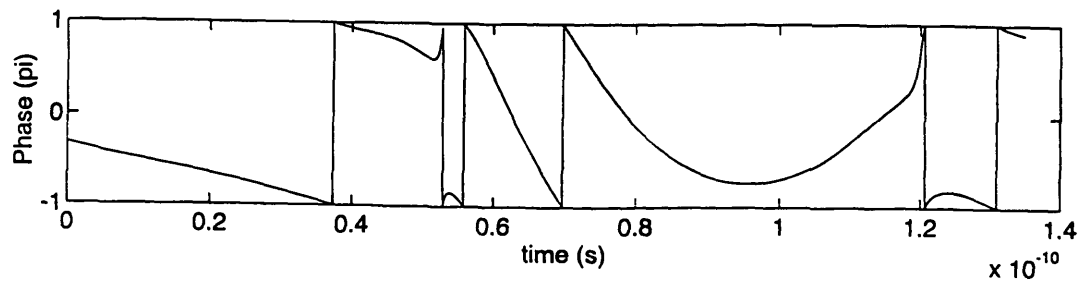


Figure 7.19. Phase corresponding to Figure 7.18.

with the lowest point in carrier density. In **Figure 7.23**, the phase of the pulse is almost linear during most of the pulse, and during the smaller pulse, the phase is linear although it is difficult to tell with such a steep slope. The phase is slightly positively inclined signifying a small positive phase shift which can be noticed in the frequency spectrum (**Figure 7.21**). The pulse width is 12.6ps although it would probably a little bit smaller once it reaches steady-state. The spectrum of an entire roundtrip of time is rather messy because the spectrums of the two pulses combine in this way, but if the small pulse is manually removed, the spectrum is clean looking. The bandwidth of this spectrum is .0795THz.

The best looking pulses came from a simulation with even less dispersion, $D_{fb}=7.106 \times 10^{-27} \text{s}^2$ (**Figure 7.24**). However, the larger pulse is shrinking slowly, and the peak of the pulse is shifted far after the peak of the carrier density. The phase of a single pulse is not as linear as the above simulations although it has bit less chirp than without any dispersion if compared to **Figure 7.14**. The smaller pulse also seems to have only a small amount of chirp. The one very nice thing about these results is that the intensity of the pulse is almost as high as it should be and still has very little chirp. There is a significant amount of frequency shift as can be seen in the phase plot and the spectrum plot (**Figure 7.25 and 27**). The pulsewidth is 7.4ps and the bandwidth is .0789THz.

Portions of this work were performed at the Cornell Theory Center, supported in part by the National Science Foundation, by the IBM Corporation, by the New York State Science and Technology Foundation, and by the Corporate Research Institute.

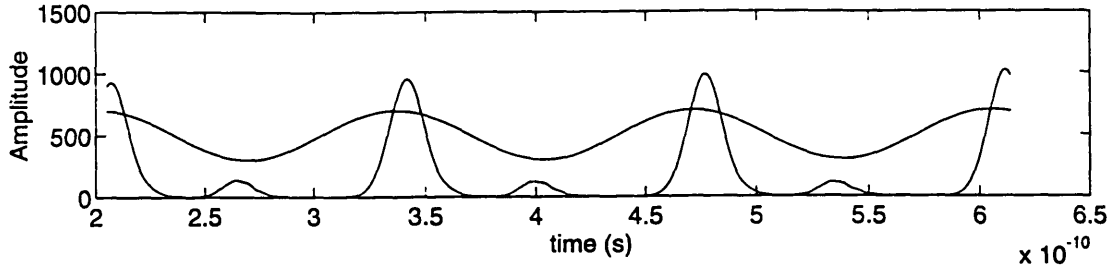


Figure 7.20. Series of pulses from simulation with $D_{fb}=2.5332 \times 10^{-26}$ and $a=5$. Sinusoidal line is relative carrier density (not actual values).

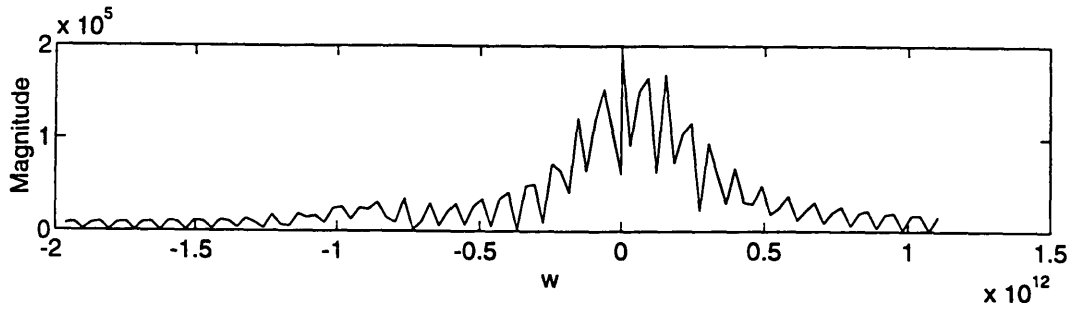


Figure 7.21. Frequency spectrum of a single pulse from the above series.

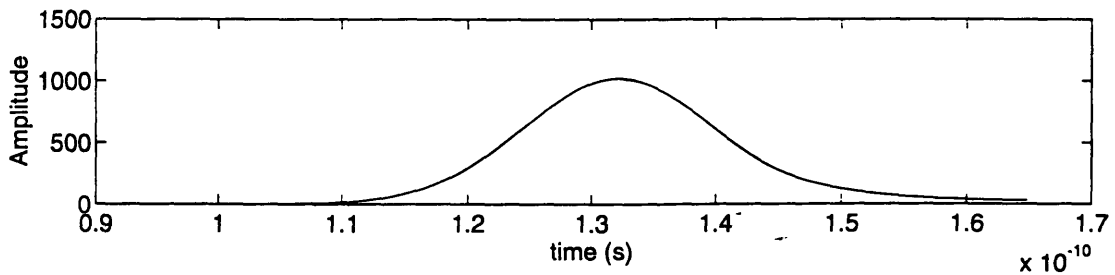


Figure 7.22. Single pulse from simulation with $D_{fb}=2.5332 \times 10^{-26}$ and $a=5$.

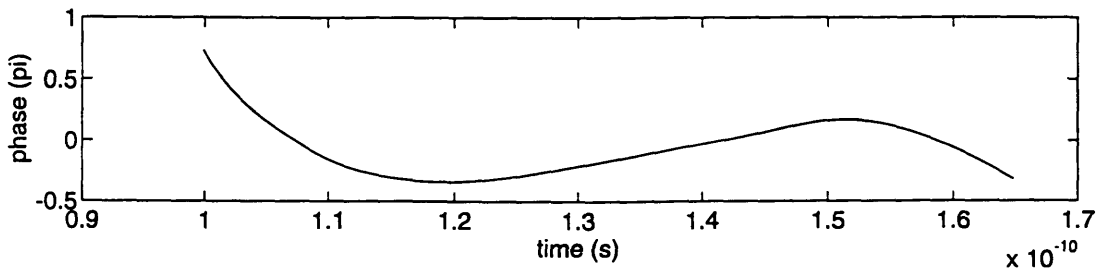


Figure 7.23. Phase corresponding to Figure 7.22.

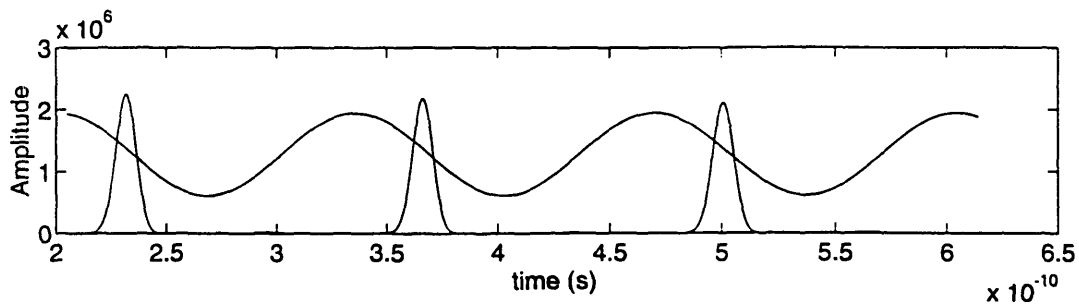


Figure 7.24. Series of pulses from simulation with $D_{fb}=7.1061 \times 10^{-27}$ and $a=5$. Sinusoidal line is relative carrier density (not actual values).

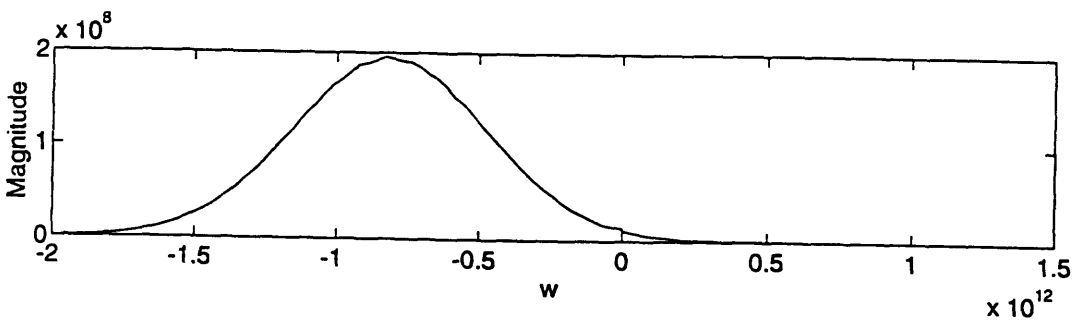


Figure 7.25. Frequency spectrum of a single pulse from the above series.

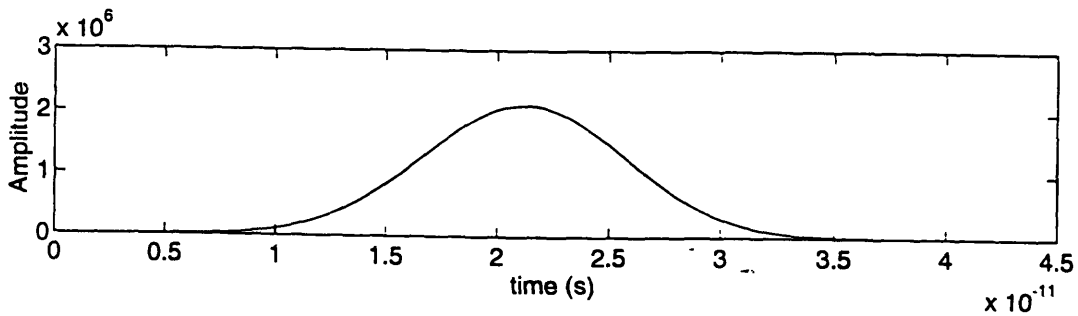


Figure 7.26 Single pulse from simulation with $D_{fb}=7.1061 \times 10^{-27}$ and $a=5$.

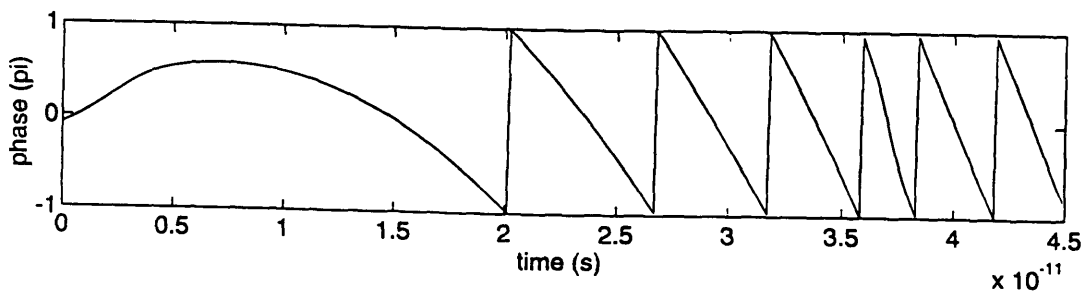


Figure 7.27. Phase corresponding to Figure 7.26.

Chapter 8

Conclusion

8.1 Summary of Results

Just to summarize some of the previous findings, **Table 8.1** reviews all of the pulsewidths and bandwidths of the pulses.

Table 8.1. Summary of values found in simulations.

D_{fb}	α	$\Delta t(\text{ps})$	$\Delta\nu(\text{THz})$	$\Delta t\Delta\nu$
0	0	7	.0592	.4144
0	5	5.2	.0987	.5132
1.2662e-25	5	20.6	.00987	.2033
2.5332e-26	5	12.6	.0796	1.003
7.1061e-27	5	7.4	.0789	.5839

8.2 Analysis of Results

There must be a reason for the double pulsing. From the *Excel* calculations, it was noticed that for increasing dispersion was also increasing δT . If the pulse shifts too far on the late side of the gain curve then it is possible for a pulse to grow on the early side. Once this happens, the growing pulse saturates the medium for the later pulse, and all of the theory falls apart. If the modulation current is increased, the double pulsing becomes worse because there is more energy for the second pulse to grow on. Maybe there is some way to cancel the time shift as well, and then the double pulsing would be prevented. However, looking at the plot of the series of pulses for the least amount of dispersion, the pulse is shifted far off the peak of the

carrier density and yet has a very small second pulse. Perhaps if the program were to run longer it would become significantly large. In any case, the pulse definitely takes longer to mode-lock with the DFB structure than without it. If one had to choose among the three simulations, the middle dispersion, $D_{fb}=2.5332 \times 10^{-26}$ seems the most promising. The chirp of the second simulation is much less than that of the third, and the pulse is not too bad and seems to be getting better.

On the other hand, it has been demonstrated that the DFB structure can be used for its dispersion to cancel the chirp due to nonlinearities in the diode. The first simulation has a very straight phase proving the lack of chirp even though double pulsing was significant.

Another plus is that the coupling coefficient can be a reasonable value for the amount of dispersion needed to compensate chirp. This was a large concern initially that happily turned out not to be any problem.

Another positive issue is that a program was written that could simulate a diode and DFB structure very well. Both can handle forward and backward waves. It is also possible to study spatial hole burning with this program since it divides the diode up into small slices and calculates the carrier density for each one independently.

8.3 Possible Improvements

The first most obvious task is to find a way to prevent the double pulsing. Perhaps modulating the current in a different way would do it, but then all of the theoretical analysis would have to be rewritten. Once this problem is understood, the model can be changed. The program is capable of handling forward and backward waves, so it would be interesting to remove the modelled isolator on one side of the diode and have a colliding pulse mode-locking ring, or a straight cavity. Ultimately, it would be possible to model a passive mode-locking system which was the original intent of this thesis. The work done for this thesis proves that it is possible to compensate for nonlinearities in the diode using a DFB structure, but much more research needs to be done to find all the ways to exploit this and to figure out how to design the best system. But before any of this, would somebody please figure out a way to make my program run faster!

8.4 The End

Appendix A

Calculating Parameters of the Pulse and DFB

Following are the spreadsheets from *Excel*, used to find values for the pulse parameters given mode-locking conditions. The equations used for these spreadsheets are all explained in Chapter 6. The above half defines the diode and DFB specifications, current, and calculates the gain and saturation terms. The bottom half calculates the unknowns from the master equation and some parameters of the DFB.

The first spread sheet is for $D_{fb}=1.2662 \times 10^{-25} s^2$; the second is for $D_{fb}=2.5332 \times 10^{-26} s^2$; and the third is for $D_{fb}=7.1061 \times 10^{-27} s^2$.

The variables in the spreadsheet look a little different than in the rest of the paper. Just in case there is confusion:

$$\beta_c = Bc$$

$$\tau = \text{tau}$$

$$|A|^2 = |A|^2$$

$$\Delta\omega = \text{del}\omega$$

$$\delta T = \text{del}T$$

$$\psi = \text{psi}$$

Diode Specifications		Carrier Density		DFB specs	
go	5.00E-20	Ndc	1.5556E+24	length (m)	0.01
te	2.20E-09	Nac	1.4031E+23	length (cm)	1
tp	1.60E-12	Nmax	1.6959E+24	vg m/s	75000000
vg	7.50E+07	G	0.07892165	vg cm/s	7500000000
gamma	0.3			k cm-1	250
wg	6.28318E+12	Saturation Terms			
Nt	1.00E+24	Gm	1.0902E+17		
alpha	5	S1	2.1342E-19	Dfb for no chirp:	1.2662E-25
wo	1.44996E+15	S2	4.8831E-08	B'' s2/cm	2.5324E-25
beta''	8.96574E-25	S3	-11.097886	B''' s3/cm	-6.2591E-38
Current Values		loss	0.02	delo	-1656.08629
ld	0.003393939			wb	1.4624E+15
lac	0.0315	tau	3.4803E-12		
		width	8.1954E-12	ratio	-0.1894946
Diode Dimensions					-0.06316487
length	7.50E-05	Dd	3.3622E-29		
a _{eff}	4E-13				
V	3.00E-17				
Constants					
q	1.60E-19				
rndtrip time	1.34333E-10				
wm	46773052109				
Getting all the unknowns =====					
Dt=	1.26652E-25		1.27E-25		
Dt	1.27E-25			Dfb	1.27E-25
				B''	2.5324E-25
Finding B		Finding delw			
a	-2.29589E-40	a	2.533E-26		
b	1.31718E-24	b	-3.656E-15	delo	-1656.08629
c	2.29589E-40	c	-0.05683036		
				wb for wc	1.461E+15
B	0	delw	-1.4274E+12		
tau^4	1.46708E-46	A ^2	2.4453E+16	wb for wo	1.4624E+15
tau	3.48027E-12	delT	-3.4711E-13		
width	8.19542E-12	psi	0.59547185	wc	1.4485E+15
B-	5.73712E+15				
	-4.82882E-15			ratio	-0.1894946

Diode Specifications		Carrier Density		DFB specs	
go	5.00E-20	Ndc	1.5556E+24	length (m)	0.01
te	2.20E-09	Nac	1.4031E+23	length (cm)	1
tp	1.60E-12	Nmax	1.6959E+24	vg m/s	75000000
vg	7.50E+07	G	0.07892165	vg cm/s	7500000000
gamma	0.3			k cm-1	250
wg	6.28318E+12	Saturation Terms			
Nt	1.00E+24	Gm	1.0902E+17		
alpha	5	S1	2.1342E-19	Dfb for no chirp	1.2662E-25
wo	1.44996E+15	S2	4.8831E-08	B" s2/cm	2.5324E-25
beta"	8.96574E-25	S3	-11.097886	B''' s3/cm	-6.2591E-38
Current Values:					
ld	0.003393939	loss	0.02	delo	-1656.08629
lac	0.0315	tau	3.4803E-12	wb	1.4624E+15
		width	8.1954E-12	ratio	-0.1894946
Diode Dimensions					
length	7.50E-05	Dd	3.3622E-29		-0.06316487
a _{eff}	4E-13				
V	3.00E-17				
Constants					
q	1.60E-19				
rndtrip time	1.34333E-10				
wm	46773052109				
Getting all the unknowns =====					
Dt=	1.26652E-25		2.53E-26		
Dt	2.53E-26			Dfb	2.53E-26
				B"	5.0593E-26
Finding B					
a	1.01321E-25	a	2.533E-26		
b	3.03964E-25	b	-6.4242E-15	delo	-2811.54366
c	-1.01321E-25	c	-0.05627176		
				wb for wc	1.4697E+15
B	0.302775638	delw	-1.3691E+12		
tau^4	4.44196E-47	A ^2	4.1211E+16	wb for wo	1.4711E+15
tau	2.58163E-12	delT	-7.6945E-14		
width	6.07927E-12	psi	0.40354615	wc	1.4486E+15
B-	-3.302775638				
	-4.84543E-46			ratio	-0.14821453

Diode Specifications		Carrier Density		DFB specs	
go	5.00E-20	Ndc	1.5556E+24	length (m)	0.01
te	2.20E-09	Nac	1.4031E+23	length (cm)	1
tp	1.60E-12	Nmax	1.6959E+24	vg m/s	75000000
vg	7.50E+07	G	0.07892165	vg cm/s	7500000000
gamma	0.3			k cm-1	400
wg	6.28318E+12	Saturation Terms			
Nt	1.00E+24	Gm	1.0902E+17		
alpha	5	S1	2.1342E-19	Dfb for no chirp	1.2662E-25
wo	1.44996E+15	S2	4.8831E-08	B'' s2/cm	2.5324E-25
beta''	8.96574E-25	S3	-11.097886	B''' s3/cm	-4.5946E-38
Current Values		loss	0.02	delo	-2274.97322
ld	0.003393939	tau	3.4803E-12	wb	1.467E+15
lac	0.0315	width	8.1954E-12	ratio	-0.13910098
Diode Dimensions					-0.04636699
length	7.50E-05	Dd	3.3622E-29		
aeff	4E-13				
V	3.00E-17				
Constants					
q	1.60E-19				
rndtrip time	1.34333E-10				
wm	46773052109				
Getting all the unknowns =====					
Dt=	1.26652E-25		1.27E-25		
Dt	7.11E-27		7.1061E-27	Dfb	7.07E-27
				B''	1.4145E-26
Finding B		Finding delw			
a	1.19546E-25	a	2.533E-26		
b	1.21722E-25	b	-4.9133E-15	delo	-5872.30334
c	-1.19546E-25	c	-0.05565054		
				wb for wc	1.4926E+15
B	0.613032343	delw	-1.3884E+12		
tau^4	4.11126E-47	A ^2	3.1964E+16	wb for wo	1.494E+15
tau	2.53218E-12	delT	-5.2844E-14		
width	5.96282E-12	psi	0.41664055	wc	1.4486E+15
B-	-1.631235305				
	-1.09398E-46			ratio	-0.07211061

Appendix B

The Program

Mode-Locked Semiconductor Diode Simulator--Ring Model with DFB structure

c Description:

- c This program simulates a semiconductor diode in a mode-locked state of a ring model. The ring consists of the diode and a DFB structure which the program also simulates. The DFB structure may or may not have matched ends.
- c Given parameters include diode specifications, DFB parameters, current values (dc and ac).
- c Input is given within the program by "feed" array that has initial input pulse.
- c Output is two arrays of a number of pulses (depending on modulation frequency). First array is last 400ps going into diode, and second array is last 400ps coming out of diode.(Or switched)

```
program nwring3
```

```
integer lim,tot,half,off,j,fld,orig,time,numslabs,numflds
integer limtime,quad,flag
real*8 fftscale,len,taup,taus,g,aeff,Nt,q,V,width,delt,tu,vg
real*8 N(35),ma,sj1,sj,Icj,Icj1,Ic,k1,k2,k3,k4,nma,phase,li
real*8 neff,pi,beta0,beta1,beta2,w,wo,c,carr(6200)
real*8 mb,sb,sa,nmb,runtime,alpha,delg,Non,loss
real*8 aux1(20000),aux2(20000),feed(4096)
complex*16 i,Prop(0:2047),at(35)
complex*16 a(1:35,0:2047),in(6200),out(6200),Nonx(35)
complex*16 b(1:35,0:2047),bt(35)
complex*16 reflect(0:2047),transfer(0:2047),x(0:2047)
```

```
data i /(0.d0,-1.d0)/, pi /3.1415927d0/
```

```
call xufLOW(0)
```

```
lim=2047
```

```
tot=lim+1
```

```
fftscale=1.d0/tot
```

```
c Length of diode and diode sections
```

```
len=7.5000002d-6*17.d0
```

```
li=7.5d-6
```

```
numslabs=int(len/li)
```

```
numflds=numslabs+1
```

```
orig=5
```

```
print*,numslabs
```

```
c Call to DFB
```

```
flag=0
```

```
call dfbjay(orig,transfer,reflect,flag)
```

```
c Diode Specifications
```

```
taup=1.6d-12
```

```
taus=2.2d-9
```

```
g=2.5d-20*1.d0
```

```
gamma=.3d0
```

```
aeff=2.d-6*.2d-6
```

```
Nt=1.d24
```

```
q=1.6d-19
```

```
V=len*aeff
```

```
loss=dexp(-0.004d0)
```

```
c Initial pulse and time parameters
```

```
width=15.d-12
```

```

tu=width*width/4.d0/dlog(2.d0)
delt=1.d-13
half=(lim-1)/2
quad=(lim+1)/4
neff=4.d0
c=3.d8
vg=c/neff

```

c Runtime

```

runtime=2048.d-13*20.d0
limtime=int(runtime/delt)

```

c Frequency and Diode Propagation parameters

```

wo=2*pi*c/1.3d-6
delw=2*pi/tot/delt
beta0=0
beta1=1/vg

```

```

c beta2=0.6d6*pi/wo/wo
beta2=0
alpha=5

```

c Propagation array

```

do 10 j=0,lim
  if (j.le.(lim+1)/2) then
    w=j*delw
  else
    w=(j-lim-1)*delw
  end if
  Prop(j)=cdexp(-i*(beta0+w*beta1+w*w*beta2)*li)
10 continue

```

```

call propag(Prop,orig,x)

```

c Initializing Arrays

```

do 20 fld=1,numflds
do 30 j=0,lim
a(fld,j)=0
b(fld,j)=0
30 continue
20 continue

c Initial Pulse
do 40 j=0,2*tot
feed(j)=0
c feed(j)=dexp(-(delt*(j-tot)*delt
c & *(j-tot))/tu)*1.d-3
40 continue

c Initial Carrier Density
do 50 fld=1,numslabs
c N(fld)=15.20d-3*taus/q/V
N(fld)=Ic(0,len)/q/V
50 continue
print*,N(1)

c @@@@ Beginning of time step @@@@
do 60 time=1,limtime

if (time.le.6200) then
in(time)=a(1,orig)
else
do 52 j=1,6199
in(j)=in(j+1)
52 continue
in(6200)=a(1,orig)
end if

Icj=Ic(time-1,len)

```



```

c    as(fld,j)=at*x(j)
c    bs(fld,j)=bt*x(j)
c100 continue

```

```

c ***** Nonlinear Effect *****
      Non=alpha*delg*0.5d0
      Nonx(fld)=dcos(li*Non)+i*dsin(li*Non)
c *****

```

```

70  continue

```

```

c %%% End of Slab step through %%%

```

```

c Propagation through diode:

```

```

      do 110 fld=1,numslabs
        do 120 j=0,lim
          a(fld+1,j)=a(fld+1,j)+at(fld)*x(j)
          b(fld,j)=b(fld,j)+bt(fld)*x(j)
        120  continue
      110  continue

```

```

c Advancing each array

```

```

      do 130 fld=1,numflds
        do 140 j=0,lim
          a(fld,j)=a(fld,j+1)
          b(fld,j)=b(fld,j+1)
        140  continue
        a(fld,lim)=0
        b(fld,lim)=0
      130  continue

```

```

c Completing Nonlinearity

```

```

      do 142 fld=1,numslabs

```



```
& cdabs(out(j)),cdabs(in(j)),carr(j)
200 continue
```

```
c do 65 j=1,512
c & cdabs(in(j)),cdabs(out(j))
c65 continue
```

```
end
```

```
c ***** CURRENT *****
```

```
function Ic(time,len)
```

```
integer time,off,half
```

```
real*8 tau,delt,It,len,Ic,sub,tr,wm,Iac,taus
```

```
taus=2.2d-9
```

```
tr=101.65d-12
```

```
wm=2.d0*3.1415927d0/tr
```

```
half=4096
```

```
off=250
```

```
delt=1.d-13
```

```
It=7.9d-3
```

```
tau=3185.d-14
```

```
c Iac=85.d-3
```

```
Iac=0
```

```
Ic=Iac*dcos(wm*(time-half+off)*delt)+It
```

```
if (time.eq.0) Ic=It*taus+Iac/wm*dcos(wm*delt*(-half+off))
```

```
c Ic=(100.d0*dexp(-(delt*(time-half+off)*delt*(time-half+off))
```

```
c &    /(2*tau*tau))*1.d-3+It)*len/250.d-6
```

```
end
```

```
c ***** PHASE *****
```

```
function phase(arg)
```

```
real*8 rp,ip
```

```
complex*16 arg
```

```
rp=dreal(arg)
```

```
ip=dimag(arg)
```

```
if ((rp.eq.0).and.(ip.eq.0)) then
```

```
  phase=0.d0
```

```
else
```

```
  phase=datan2(ip,rp)
```

```
end if
```

```
end
```

```
c %%%%%%%%% Propagation Routine %%%%%%%%%
```

```
subroutine propag(Prop,orig,a)
```

```
integer j,orig,lim,tot
```

```
real*8 aux1(20000),aux2(20000),fftscale
```

```
complex*16 Prop(0:2047),a(0:2047),af(0:2047)
```

```
lim=2047
```

```
tot=lim+1
```

```
fftscale=1.d0/tot
```

```
do 10 j=0,lim
```

```

a(j)=0
10  continue

a(orig)=1

call dcft(1,a(0),1,tot,af(0),1,tot,tot,1,-1,1.d0,
&      aux1,20000,aux2,20000)
call dcft(0,a(0),1,tot,af(0),1,tot,tot,1,-1,1.d0,
&      aux1,20000,aux2,20000)

do 98 j=0,lim
af(j)=af(j)*Prop(j)
98  continue

call dcft(1,af(0),1,tot,a(0),1,tot,tot,1,1,fftscale,
&      aux1,20000,aux2,20000)
call dcft(0,af(0),1,tot,a(0),1,tot,tot,1,1,fftscale,
&      aux1,20000,aux2,20000)

end

c $$$$$$$$$$ DFB SECTION $$$$$$$$$$$$$$$$$$$$$$

subroutine dfbjay(orig,ao,bz,flag)

integer j,lim,tot,half,flag,orig
real*8 fftscale,delt,pi,delw,wo,c,neff,vg,delo,wb
real*8 w,aux1(20000),aux2(20000),L,arg,wg,wx,width,band
real*8 betao,lo,phi,period,p,dfbloss,k
complex*16 i,az(0:2047),azf(0:2047),bo(0:2047),bof(0:2047)
complex*16 beta,s(2,2),ao(0:2047),aof(0:2047),bz(0:2047),cdcosh

```

```
complex*16 bzf(0:2047),del,ques(0:2047),ansin,ancos,cdsinh  
complex*16 axsin,axcos,sx(2,2),sg(2,2),s1(2,2),s2(2,2),id(2,2)
```

```
data i /(0.d0,-1.d0)/, pi /3.1415927/
```

```
call xuflow(0)
```

```
c flag=0
```

```
id(1,1)=1
```

```
id(1,2)=0
```

```
id(2,1)=0
```

```
id(2,2)=1
```

```
lim=2047
```

```
tot=lim+1
```

```
fftscale=1.d0/tot
```

```
width=15.d-12
```

```
wg=pi*2.0d0/width
```

```
wx=wg*14
```

```
c wx=2*pi*1012
```

```
print*,wx
```

```
delt=1.d-13
```

```
delw=2.d0*pi/delt/tot
```

```
half=(lim-1)/2
```

```
wo=2*pi*3.d8/1.3d-6
```

```
c=3.d8
```

```
c Impulse Initialization
```

```
do 10 j=0,lim
```

```
az(j)=0
```

```
if (j.eq.orig) az(j)=1
```

```
bo(j)=0
```

10 continue

c DFB parameters

neff=3.d0

vg=c/neff

c k=20000.d0

k=0

L=.01

delo=110000.d0

wb=wo-delo*c/neff

betao=sqrt(delo*delo-k*k)

c lo=(1/betao)*(dasin(betao*(delo-betao)/(k*k*sqrt(1-(delo-betao)

c & *(delo-betao)/(k*k))))

phi=pi/2-datan(delo*dtan(betao*lo)/betao)

period=pi*vg/wb

p=phi*3.d10/2.d0/wo

dfbloss=1.d0

call dcft(1,az(0),1,tot,azf(0),1,tot,tot,1,-1,1.d0,aux1,20000,
& aux2,20000)

call dcft(0,az(0),1,tot,azf(0),1,tot,tot,1,-1,1.d0,aux1,20000,
& aux2,20000)

call dcft(1,bo(0),1,tot,bof(0),1,tot,tot,1,-1,1.d0,aux1,20000,
& aux2,20000)

call dcft(0,bo(0),1,tot,bof(0),1,tot,tot,1,-1,1.d0,aux1,20000,
& aux2,20000)

do 100 j=0,lim

if (j.le.(lim+1)/2) then

w=j*delw

```

else
  w=(j-lim-1)*delw
end if

del=(w+wo-wb)/vg
arg=k*k-del*del
c
band=dexp(-w*w/wx/wx)
azf(j)=azf(j)*band

if (arg.lt.0.d0) then
  beta=i*dsqrt(-1.d0*arg)
else
  beta=dsqrt(arg)
end if
c

ansin=cdsinh(L*beta)
ancos=cdcosh(L*beta)
c  print*, 'ansin', j, ansin
c  print*, 'ancos', j, ancos

s(1,1)=ancos+i*del/beta*ansin
s(1,2)=i*k/beta*ansin
s(2,1)=-i*k/beta*ansin
s(2,2)=ancos-i*del/beta*ansin

c If using matching structure
if (flag.eq.1) then

  axsin=cdsinh(lo*beta)
  axcos=cdcosh(lo*beta)
  sx(1,1)=axcos+i*del/beta*axsin
  sx(1,2)=i*k/beta*axsin

```



```
sx(2,1)=-i*k/beta*axsin
sx(2,2)=axcos-i*del/beta*axsin
```

```
sg(1,1)=cdexp(i*w*p/c)
sg(1,2)=0
sg(2,1)=0
sg(2,2)=cdexp(-i*w*p/c)
```

```
call mulmat(sg,sx,s1,1)
call mulmat(s,s1,s2,1)
call mulmat(sg,s2,s1,1)
call mulmat(sx,s1,s,1)
```

```
end if
```

```
aof(j)=azf(j)/s(1,1)-s(1,2)/s(1,1)*bof(j)
bzf(j)=azf(j)*s(2,1)/s(1,1)+(s(2,2)-s(1,2)*s(2,1)/s(1,1))
& *bof(j)
```

```
band=dexp(-w*w/wx^2)
aof(j)=aof(j)*band
```

```
100 continue
```

```
call dcft(1,aof(0),1,tot,ao(0),1,tot,tot,1,1,fftscale,aux1,
& 20000,aux2,20000)
call dcft(0,aof(0),1,tot,ao(0),1,tot,tot,1,1,fftscale,aux1,
& 20000,aux2,20000)
call dcft(1,bzf(0),1,tot,bz(0),1,tot,tot,1,1,fftscale,aux1,
& 20000,aux2,20000)
```

```

        call dcft(0,bzf(0),1,tot,bz(0),1,tot,tot,1,1,fftscale,aux 1,
&          20000,aux2,20000)

c   open(unit=13,file='dfbjpul1',status='old')
c   do 150 j=0,lim
c   write(13,'(1x,4e14.5)') delt*(j-half),cdabs(az(j)),
c   &      cdabs(az(j)), cdabs(bz(j))
c150 continue

        end

c *****          cdcosh *****

        function cdcosh(arg)

        complex*16 arg, cdcosh

        if (dreal(arg).gt.83) then
            cdcosh=1.d36
        else
            cdcosh=(cdexp(arg)+cdexp(-1.d0*arg))/2
        end if
        end

c *****          CDSINH *****

        function cdsinh(arg)

        complex*16 arg, cdsinh,i
        data i /(0.d0,-1.d0)/

        if (dimag(arg).eq.0.d0) then
            if (dreal(arg).gt.83) then

```

```

    cdsinh=1.d36
else
    cdsinh=(cdexp(arg)-cdexp(-1.d0*arg))/2
end if
else
    cdsinh=i*dsin(cdabs(arg))
end if

end

```

c \$\$\$\$\$\$\$\$\$\$\$\$ subroutine mulmat \$

```

subroutine mulmat(trix1,trix2,matrix,n)

```

- c Multiplies two matrices: n=1 answer in matrix
- c Also raises trix1 to the nth power: trix2 is the identity matrix

```

integer n,j
complex*16 trix1(2,2),trix2(2,2),matrix(2,2)

```

```

do 100 j=1,n
matrix(1,1)=trix1(1,1)*trix2(1,1)+trix1(1,2)*trix2(2,1)
matrix(2,1)=trix1(2,1)*trix2(1,1)+trix1(2,2)*trix2(2,1)
matrix(1,2)=trix1(1,1)*trix2(1,2)+trix1(1,2)*trix2(2,2)
matrix(2,2)=trix1(2,1)*trix2(1,2)+trix1(2,2)*trix2(2,2)

```

c print*, 'matrix in mulmat:', matrix

```

if (n.gt.1) then
trix2(1,1)=matrix(1,1)
trix2(1,2)=matrix(1,2)
trix2(2,1)=matrix(2,1)
trix2(2,2)=matrix(2,2)
endif

```

```
100 continue  
    return  
end
```

References

- [1] K. L. Hall, "Femtosecond Nonlinearities in InGaAsP Diode Lasers," MIT thesis, May 1993.
- [2] H. A. Haus, "A Theory of Forced Mode Locking," IEEE J. Quantum Electron. **11**, 323 (1975)
- [3] G. P. Agrawal and N. K. Dutta, *Long-Wavelength Semiconductor Lasers*, Van Nostrand Reinhold Company, Inc., 1986.
- [4] C. H. Henry, "Theory of the Linewidth of Semiconductor Lasers," IEEE J. Quantum Electron. **18**, 259 (1982)
- [5] C. H. Henry, R. A. Logan, and K. A. Bertness, "Spectral dependence of the change in refractive index due to carrier injection in GaAs lasers," J. Appl. Phys. **52**, 4458 (1981)
- [6] H. A. Haus, "Matching of distributed-feedback structures," Opt. Lett. **17**, 1134 (1992)
- [7] H. A. Haus, *Waves and Fields in Optoelectronics*, Englewood Cliffs, NJ: Prentice-Hall, Inc., 1984.
- [8] Numerical Recipes in Fortran
- [9] J. N. Damask, "A New Photonic Device: The Integrated Resonant Channel-Dropping Filter," MIT thesis, May 1993.
- [10] H. A. Haus, "Modelocking of Semiconductor Laser Diodes," Japanese Journal of Applied Physics. **20**,1007 (1981).

Background References

- H. A. Haus, J. G. Fujimoto, and E. P. Ippen, "Structures for additive pulse mode locking," J. Opt. Soc. Am. B **8**, 2068 (1991)
- H. A. Haus, "Mode-locked Semiconductor Diode Lasers," Philosophical Transactions of the Royal Society of London A. **298**, 257 (1980).
- J. C. Chen, H. A. Haus, and E. P. Ippen, "Stability of Lasers Mode Locked by Two Saturable Absorbers," IEEE J. Quantum Electron. **29**, 1228 (1993)
- H. A. Haus, "Theory of Mode Locking with a Slow Saturable Absorber," IEEE J. Quantum Electron. **11**, 736 (1975)

M. Osinski, and J. Buus, "Linewidth Broadening Factor in Semiconductor Lasers--An Overview," *IEEE J. Quantum Electron.* **23**, 9 (1987)

J. C. Chen, "Theory of Passively Mode-locked Lasers with Dynamic Gain Saturation," MIT thesis, August 1991.

G. P. Agrawal, *Nonlinear Fiber Optics*, San Diego, CA: Academic Press, 1989.

R. J. Deri, and E. Kapon, "Low-Loss III-V Semiconductor Optical Waveguides," *IEEE J. Quantum Electron.* **23**, 626 (1991)

T. Saitoh, and T. Mukai, "Traveling-Wave Semiconductor Laser Amplifiers," *Coherence, Amplification, and Quantum Effects in Semiconductor Lasers*, edited Y. Yamamoto, John Wiley & Sons, Inc., 1991.

I. Organos, T. Sphicopoulos, A. Tsigopoulos, and C. Caroubalos, "A Tractable Above-Threshold Model for the Design of DFB and Phase-Shifted DFB Lasers," *IEEE J. Quantum Electron.* **27**, 946 (1991)

H. A. Haus, "Grating Filter Transformation Chart," *Electronics Letters* **11**, 553 (1975)